RESOURCE GEOLOGY

doi: 10.1111/j.1751-3928.2011.00180.x *Resource Geology* Vol. 62, No. 1: 63–83

Thematic Article

Major and Trace Element Characteristics of Apatites in Granitoids from Central Kazakhstan: Implications for Petrogenesis and Mineralization

Mingjian Cao,[1,2] Guangming Li,[1] Kezhang Qin,[1] Eleonora Yusupovha Seitmuratova[3] and Yongsheng Liu[4]

[1]*Key Laboratory of Mineral Resources, Institute of Geology and Geophysics, Chinese Academy of Sciences,* [2]*Graduate University of Chinese Academy of Sciences, Beijing, China,* [3]*K. Satpaev Institute of Geological Sciences, Almaty, Republic of Kazakhstan and* [4]*State Key Laboratory of Geological Processes and Mineral Resources, Faculty of Earth Sciences, China University of Geosciences, Wuhan, China*

Abstract

This paper presents abundances of major and trace elements of apatites in granitic rocks associated with different types of ore deposits in Central Kazakhstan on the basis of electron probe microanalysis and laser ablation inductively coupled plasma mass spectrometry. Our results demonstrate that the concentrations and ratios of elements in apatites from different granitoid rocks show distinct features, and are sensitive to magma evolution, petrogenetic and metallogenetic processes. Apatites in the rocks associated with Mo-W deposits have high content of F and MnO, low content of Cl, which may be indicative of sedimentary sources, while apatites from a Pb-Zn deposit show relatively high content of Cl and low F content, which possibly suggest a high water content. In these apatites, Sr contents decrease, while Mn and Y contents increase with magma evolution. This relationship reflects that these elements in apatites are related with the degree of magmatic differentiation. Four types of REE patterns in apatites are identified. Type 1 character of highest $(La/Yb)_N$ in apatites of Aktogai porphyry Cu-Mo deposit, Sayak-I skarn Cu deposit and Akzhal skarn Pb-Zn depposit is likely produced by the crystallization of heavy REE-enriched minerals. Type 2 character of upward-convex light REE in apatite of Aktogai porphyries likely results from La-enriched mineral crystallization. Type 3 feature of Nd depletion in apatites of East Kounrad and Zhanet deposits both from Mo-W deposits primarily inherits the character of host-rock. Type 4 apatites of Aktogai deposit and Akshatau W-Mo deposit with wide range of REE contents may suggest that apatites crystallize under a wide temperature range. Three types of apatite with distinct redox states are identified based on Eu anomaly. The Aktogai apatite with slight negative Eu anomaly displays the most oxidized state of the magma, and the apatites of other samples at Aktogai, East Kounrad and Akzhal with moderate negative Eu anomaly show moderate oxidizing condition of these rocks, while the remaining apatites with strong En anomaly indicate a moderate reductive state of these rocks.

Keywords: apatite, Central Kazakhstan, granitoid, magmatic differentiation, metallogenetic processes, redox states.

Received 27 May 2010. Accepted for publication 16 October 2011.
Corresponding author: G. LI, Key Laboratory of Mineral Resources, Institute of Geology and Geophysics, Chinese Academy of Sciences, P.O. Box 9825, Beijing 100029, China. Email: lgm@mail.iggcas.ac.cn

1. Introduction

Apatite, $Ca_5(PO_4)_3(OH,F,Cl)$, is the most abundant phosphate in igneous rocks. Because of several substitutions in both anion and cation sites, apatite contains many elements, such as halogens (F, Cl), sulfur (S), strontium (Sr), uranium (U), thorium (Th), rare earth elements (REEs) and thus could be used for radiometric dating (e.g. Zeitler *et al*., 1987; McInnes *et al*., 1999; Farley & Stockli, 2002; Harrison *et al*., 2002), fission track dating (e.g. Omar *et al*., 1987; Gleadow *et al*., 2002; Hasebe *et al*., 2004), chloride and fluoride composition calculation, halogen fugacity determination (e.g. Korzhinskiy, 1981; Zhu & Sverjensky, 1992), magma evolution processes study (e.g. Ishihara, 1981; Korzhinskiy, 1981; Nash, 1984; Hsieh *et al*., 2008; Chu *et al*., 2009), geochemical exploration (e.g. Treloar & Colley, 1996; Belousova *et al*., 2001; 2002) and temperature calculation (e.g. Munoz, 1984; Sallet, 2000). However, few works have been studied to discuss apatite as an indicator for metallogenesis and ore types (Belousova *et al*., 2001; 2002; Imai, 2002, 2004).

Central Kazakhstan (66°E–78°E, 46°N–54°N), is a unique metallogenic province characterized by its abundance of granite-related ore deposits (Fig. 1), hosts many different types of deposits, such as porphyry Cu (-Mo), skarn, greisen, quartz-vein, volcanogenic massive sulfide (VMS) Cu-Pb-Zn and intrusion-related Au deposits.

This paper presents major and trace elements of apatites from 12 different plutons which are associated with six different ore deposits, by using electron microprobe analysis (EMPA) and laser ablation-ICP-MS (LA-ICP-MS). The main objectives of this paper are: (i) to investigate the geochemical characteristics of these elements in apatites from different types of deposits; (ii) to propose a systematic explanation for the major and trace elements in the magmatic and hydrothermal processes; and (iii) to use the chemical composition of apatites as an indicator of the metallogenesis and ore types.

2. Tectonic setting

Central Asia Orogenic Belt (CAOB) (Mossakovsky *et al*., 1993), also known as the Altaids (Sengor, 1993; Sengor & Natal'in, 1996), extends from the Urals to the northwest Pacific and from Siberian and Baltica cratons to Sino-Korean and Tarim cratons. Several models have been proposed to explain the evolution of the CAOB, for example, a long-lived, single orogenic system (Sengor, 1993; Sengor & Natal'in, 1996), a three-arc kipchak model (Yakubchuk *et al*., 2001, 2005; Yakubchuk, 2004) and a collage of various terranes with multiple subduction systems (Coleman, 1989; Mossakovsky *et al*., 1993; Heinhorst *et al*., 2000; Qin, 2000; Qin *et al*., 2002, 2003; Xiao *et al*., 2004a, 2004b, 2009). Central Kazakhstan, located in the midwest of CAOB, has many large mineral deposits (Cu, Mo, Pb, Zn, W, Sn, REE, Zr, Nb, etc.), and exposes integrated Paleozoic strata, plutons and volcanic rocks (Fig. 1).

The strata in Central Kazakhstan are divided into three units. The first unit is the Precambrian metamorphic basement, composed of schist, gneiss, amphibolite and quartz-feldspathic schist, exposed in the north and west of Central Kazakhstan, with the most prominent unit of the Kokchetav Massif in northern Kazakhstan (e.g. Apollonov & Patalakha, 1981; Zaitsev, 1984; Claoue-Long *et al*., 1991). The second unit is Paleozoic folded sedimentary and metamorphic rocks, which change from assemblages of volcanogenic silicic rocks, terrigenous clastic rocks and carbonate rocks in Cambrian and Ordovician, to terrigenous clastic rocks or shallow marine clastic rocks in Silurian and Devonian, to volcanic rocks of dacite and rhyolite intercalated with tuff in Carboniferous, and to the basalt-rhyolite and terrestrial volcanic tuff in Permian. The third unit is widespread cover of Mesozoic and Cenozoic sandstone and mudstone.

Intrusive rocks emplaced from Proterozoic to Permian, consisting primarily of Variscan granitoid rocks. Serykh (1977, 1988, 1996) subdivided the granitoid series in foldbelts of Central Kazakhstan into early or synorogenic, and late- or post-orogenic series. Four series of volcanic and intrusive rocks were recognized by Popov (1996): pre-orogenic, early orogenic, main orogenic and late orogenic series. According to Popov (1996), most of the Cu-Mo and Au deposits in the belt are associated with pre-orogenic and early orogenic diorite-granodiorite-adamellite intrusive rocks. In contrast, stockwork and vein Mo deposits and scheelite-bearing W deposits are related to main orogenic granite and leucogranite, and polymetallic Mo-W-Be-Bi mineralization is accompanied with late orogenic leucogranitic plutons.

Several remnants of Paleozoic oceanic crust are distributed in Central Kazakhstan. Most of the ophiolites show geochemical features of fore-arc, back-arc or intra-arc oceanic crust (Avdeev, 1984; Kröner *et al*., 2007). Ophiolite belts in Central Kazakhstan typically comprise only the topmost layers of palaeo-oceanic crust, especially the deep-sea sediments and volcanic

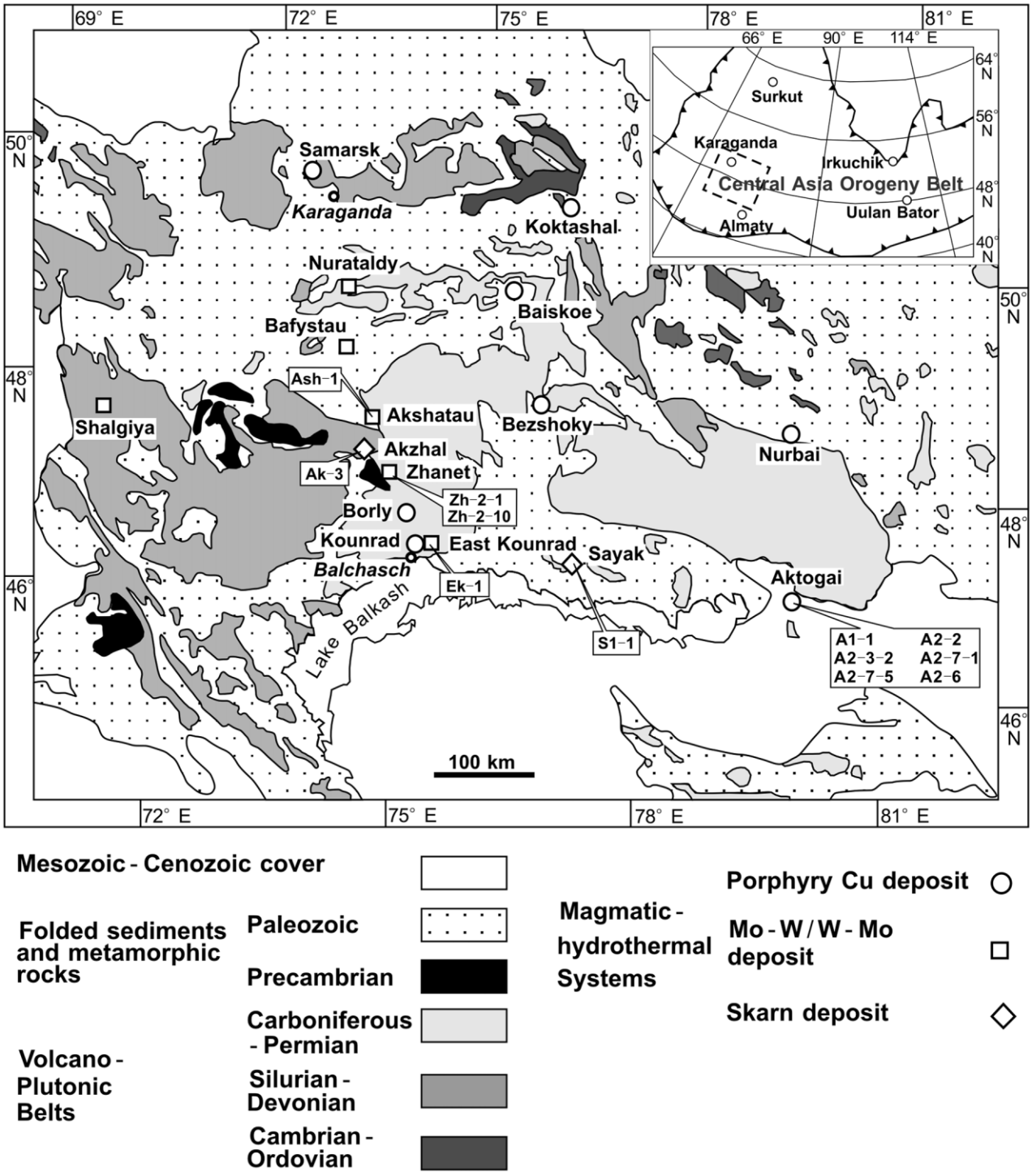

Fig. 1 Map of regional geology and ore deposits distribution of the Central Kazakhstan. Modified after Heinhorst *et al*. (2000) and Windley *et al*. (2007).

rocks. Some of the ophiolite belts host massive-sulfide Cu (-Au) deposits (Yakubchuk *et al*., 2005).

A continental environment for Central Kazakhstan after Late Ordovician and Silurian (Degtyarev, 1999; Windley *et al*., 2007) was accompanied by a magmatic arc until Carboniferous, which disappeared in Early Permian as the subduction process were completed (Zaitsev, 1984; Windley *et al*., 2007; Li *et al*., 2008).

3. Studied mineral deposit and associated rock series

Totally, 12 plutons were investigated: one batholith and five porphyries associated with porphyry Cu-Mo mineralization at Aktogai, three granitoids associated with Mo-W deposits at East Kounrad and Zhanet, one granodiorite related with skarn Cu mineralization at Sayak-I, one granite related with W-Mo deposit at Akshatau, and one diorite-porphyry associated with skarn Pb-Zn deposit at Akzhal. Details of 12 plutons are listed in Table 1. Major and trace elements of representative granitoid rocks are given in Table 2.

3.1 Aktogai porphyry Cu-Mo deposit

The Aktogai porphyry Cu-Mo deposit occurs in the Burliutobinsk region, Almaty province, 22 km east of the Aktogai railway station, and contains 3130 Mt averaging at 0.3% Cu (12.5 Mt Cu metal) (Cooke *et al*., 2005). The Cu-Mo mineralization is related with granodiorite porphyry and quartz diorite porphyry (corresponding to the sample numbers A2-2, A2-3-2, A2-6, A2-7-1, A2-7-5), and other small shallow intrusive bodies in the Early Carboniferous granodiorite batholith (A1-1), covered by Carboniferous–Lower Permian volcanosedimentary rocks. The A2-6 is relatively later in time than other porphyries based on the field observation. SIMS (secondary ion mass spectrometry) zircon ages on granodiorite (A1-1), quartz diorite porphyry (A2-3-2, A2-7-1) yielded 344.7 ± 2.9 Ma, 331.4 ± 2.6 Ma, 328.1 ± 2.1 Ma (our unpublished data). Associated hydrothermal alteration consists of silicification in the core, K-silicate alteration, quartz-sericite alteration within the stock, and propylitization in the wall-rock. The veinlet disseminated orebody mainly developed in the quartz-sericite alteration.

The values of A/CNK (Al_2O_3/[CaO + Na_2O + K_2O]) for A1-1, A2-7-5 and A2-6 are 0.92, 1.12 and 1.06, and values of A/NK (Al_2O_3/[Na_2O + K_2O]) are 1.69, 1.38 and 1.60 (Table 2), A/CNK and A/NK define the granodiorite A1-1 as metaluminous and of I-type character, while the porphyries of A2-7-5 and A2-6 as peraluminous and of transition character of I-type to S-type. The main opaque minerals found under the microscope are magnetite, pyrite and chalcopyrite, more rarely ilmenite.

3.2 Mo-W deposits and W-Mo deposit

The East Kounrad Mo-W deposit is situated 10 km to the north of the town of Balkash (Fig. 1). The ore deposit occurs in endo- and exocontact zones of syenogranite, with reserves of 200–250 kt averaging at 0.056% Mo. The age of syenogranite (EK-1) is determined at 299.7 ± 2.7 Ma by SIMS zircon method (our unpublished data). The average model age of molybdenites is 298.0 Ma for the East Kounrad Mo-W deposit (Chen *et al*., 2010).

The Zhanet Mo-W deposit is a medium-sized Mo deposit, located 120 km to the northwest of the town of Balkash (Fig. 1). The orebody occurs at the intersection of the Akzhal-Aksoran and Akbastay faults. The network Mo-W mineralization is associated with the syenogranite porphyries (Zh-2–1, Zh-2–10). Molybdenite mainly occurs in syenogranite porphyries and in late-stage quartz veins and fissures. In the late-stage quartz veins molybdenite is associated with fluorite. SIMS zircon ages on syenogranite porphyry (Zh-2–1) yielded 309.7 ± 2.7 Ma (our unpublished data), which is earlier than the ore-forming age of 295.0 Ma obtained by the average model age of molybdenite (Chen *et al*., 2010).

The Akshatau W-Mo deposit is located 150 km north-northwest of the town of Balkash (Fig. 1), in the southeastern part of the Zhaman-Sarysu Anticlinorium near its boundary with Toqrau Basin. The disseminated quartz vein-greisen type W-Mo deposit is closely related to the tops of the Carboniferous granite complex (Ash-1) in both endocontacts and exocontacts, and contains 65.5 kt of 0.10–0.30% WO_3, 17.5 kt of 0.04–0.07% Mo and 16.0 kt of 0.03–0.07% of Be (Beskin *et al*., 1996). Our unpublished 319.5 ± 3.4 Ma SIMS zircon ages seem earlier than 289.3 Ma average model age of molybdenites (Chen *et al*., 2010).

Rocks from Mo-W deposits or W-Mo deposit have evolved compositions with 70.3–76.2 wt% SiO_2 (Table 2). All three samples show I-type character with A/CNK varying from 0.96 to 1.01, though Ek-1 and Zh-2–10 from Mo-W deposits show transition characters of metaluminous to peraluminous, and Ash-1 from W-Mo deposit displays metaluminous features. The major opaque minerals are magnetite, and less molybdenite and ilmenite.

Table 1 Summary of sample localities and apatite occurrence of rocks in Central Kazakhstan

Sample	Locality	GPS position	Lithology and age (Ma)	Mineral assemblage (in volume %)	Accessory mineral phases	Apatite morphology and occurrence			
						Length (μm)	Width (μm)	Length/ width	Occurrence
A1-1	Aktogai porphyry Cu-Mo deposit	46°57′18.8″N 079°54′04.3″E	Granodiorite 344.7 ± 2.9	Pl (50%), Kfs (20%), Qtz (20%), Bt (6%), Hbl (3%), and others (1%)	Apt+Zrc+Sph	32.8–243	24.3–130	1.0–2.6	Mainly in and/or along Bio, Hbl, Mag
A2-2	Aktogai porphyry Cu-Mo deposit	46°58′06.8″N 079°59′06.3″E	Granodiorite-porphyry	Phenocrysts: Pl (55%), Kfs (15%),Qtz (20%), Bt (10%), and others (2%); and matrix: Pl, Qtz, Kfs and Bio	Apt+Zrc	36.5–300	13.1–140	1.1–4.0	Mainly as fine grained matrix intergranular apatite and included apatite in/along Bio, Mag, Pl
A2-3-2	Aktogai porphyry Cu-Mo deposit	46°58′06.8″N 079°59′06.3″E	Quartz diorite porphyry 331.4 ± 2.6	Phenocrysts: Pl (60%), Kfs (15%),Qtz (10%), Bt (12%), Hbl (3%), and others (2%); and matrix: Pl, Qtz and Bio	Apt+Zrc	—	—	—	—
A2-6	Aktogai porphyry Cu-Mo deposit	46°58′06.8″N 079°59′06.3″E	Granodiorite-porphyry	Phenocrysts: Pl (50%), Kfs (15%),Qtz (20%), Bt (10%), Hbl (3%), and others (2%); and matrix: Pl, Qtz and Kfs	Apt+Zrc	31.7–299	14.7–126	1.0–4.0	Mainly as fine grained matrix intergranular apatite and included apatite in/along Bio, Mag, Pl
A2-7-1	Aktogai porphyry Cu-Mo deposit	46°58′06.8″N 079°59′06.3″E	Quartz diorite porphyry 328.1 ± 2.1	Phenocrysts: Pl (55%), Kfs (15%),Qtz (15%), Bt (14%), and others (1%); and matrix: Pl, Qtz and Bio	Apt+Zrc	23–220	7.7–147	1.1–3.5	Mainly as fine grained matrix intergranular apatite and included apatite in/along Bio, Mag, Pl
A2-7-5	Aktogai porphyry Cu-Mo deposit	46°58′06.8″N 079°59′06.3″E	Quartz diorite porphyry	Phenocrysts: Pl (65%), Kfs (15%),Qtz (10%), Bt (10%); and matrix: Pl, Qtz and Bio	Apt+Zrc	—	—	—	—
EK-1	East Kounrad Mo-W deposit	47°01′07″N 075°08′08″E	Syenogranite 299.7 ± 2.7	Pth (50%), Qtz (35%), Pl (10%), Bt (4%) and others (1%)	Apt+Zrc	44.6–209	10.7–61.4	1.0–5.1	Mainly in Bio, Mag
Zh-2–1	Zhanet Mo-W deposit	47°31′16.7″N 074°18′55.3″E	Syenogranite porphyry 309.0 ± 2.7	Phenocrysts: Pth (40%), Qtz (40%), Pl (20%); and matrix: Qtz, Kfs and Bio	Apt+Zrc	—	—	—	—
Zh-2–10	Zhanet Mo-W deposit	47°31′16.7″N 074°18′55.3″E	Syenogranite porphyry	Phenocrysts: Pth (60%),Qtz (25%), Pl (15%); and matrix: Qtz, Pth and Bio	Apt+Zrc	—	—	—	—
S1-1	Sayak-I skarn Cu deposit	47°00′11.1″N 077°24′03.8″E	Granodiorite 311.4 ± 2.5	Pl (55%), Kfs (10%), Qtz (20%), Bt (5%), Hbl (8%), and others (2%)	Apt+Zrc+Sph	35.2–183	13.0–176	1.0–3.6	Mainly in and/or along Bio, Hbl
Ash-1	Akshatau W-Mo deposit	47°59′41.5″N 074°02′34.5″E	Granite 319.5 ± 3.4	Pl (18%), Kfs (45%), Qtz (30%), Bt (6%), and others (1%)	Apt+Zrc+Mnz+ Sph	36–242	16.4–135	1.0–4.2	Mainly in and/or along Bio, Mag
Ak-3	Akzhal skarn Pb-Zn deposit	47°44′01.1″N 073°59′22.8″E	Diorite-porphyry	Phenocrysts: Pl (85%), Hbl (15%); and matrix: Pl, Qtz, Hbl and Bt	Apt+Zrc	37.2–142	25.7–113	1.0–2.4	Mainly as fine grained matrix intergranular apatite and included apatite in/along Mag, Hbl, Bio

All the ages of plutons and porphyries are from our unpublished SIMS zircon U-Pb results.
Abbreviations for minerals: Apt, Apatite; Bt, Biotite; Hbl, Hornblende; Kfs, K-feldspar; Mag, Magnetite; Mnz, Monazite; Pth, Perthite; Pl, Plagioclase; Qtz, Quartz; Sph, Sphene; Zrc, Zircon.

Table 2 Major- and trace-elements of representative granitic rocks from Central Kazakhstan

Sample	SiO_2 (wt%)	TiO_2 (wt%)	Al_2O_3 (wt%)	Fe_2O_3 (wt%)	MnO (wt%)	MgO (wt%)	CaO (wt%)	Na_2O (wt%)	K_2O (wt%)	P_2O_5 (wt%)	LOI (wt%)	Total (wt%)
A1-1	64.6	0.59	15.0	5.28	0.11	2.20	4.09	3.21	3.31	0.12	1.42	100.0
A2-7-5	69.0	0.43	15.5	1.87	0.02	1.50	1.42	4.21	3.96	0.18	1.82	100.0
A2-6	65.1	0.57	16.5	4.26	0.02	1.58	2.91	4.38	2.86	0.24	1.88	100.3
EK-1	76.2	0.17	12.7	1.18	0.05	0.20	0.63	3.83	4.73	0.04	0.26	100.0
Zh-2–10	73.2	0.27	13.0	1.62	0.05	0.51	1.09	2.91	5.99	0.05	0.94	99.6
S1-1	65.1	0.57	15.4	4.15	0.05	2.83	3.88	4.19	3.33	0.17	0.52	100.2
Ash-1	70.3	0.35	14.4	3.03	0.08	1.16	2.85	3.51	3.82	0.10	0.28	99.9
Ak-3	58.8	0.83	16.6	7.02	0.13	2.97	5.68	3.61	2.37	0.26	2.10	100.3

Sample	V (ppm)	Sr (ppm)	Y (ppm)	La (ppm)	Ce (ppm)	Pr (ppm)	Nd (ppm)	Sm (ppm)	Eu (ppm)	Gd (ppm)	Tb (ppm)	Dy (ppm)
A1-1	128	361	19.7	15.3	30.7	4.04	16.1	3.52	0.88	3.39	0.54	3.41
A2-7-5	78.7	718	9.77	18.7	36.1	4.45	16.6	2.91	0.78	2.40	0.33	1.75
A2-6	122	923	8.25	21.2	41.3	5.47	20.1	3.62	0.87	2.51	0.31	1.55
EK-1	8.12	86.8	10.9	35.9	51.3	4.75	13.8	1.86	0.32	1.70	0.23	1.43
Zh-2–10	21.9	129	15.9	31.4	57.7	5.64	17.0	2.76	0.53	2.29	0.36	2.29
S1-1	103	696	10.9	17.5	34.7	4.38	17.0	3.24	0.90	2.63	0.38	2.12
Ash-1	52.4	288	15.2	37.3	63.1	6.44	21.2	3.36	0.71	2.90	0.43	2.56
Ak-3	135	548	21.3	30.6	57.5	6.78	25.9	5.03	1.29	4.51	0.71	3.93

Sample	Ho (ppm)	Er (ppm)	Tm (ppm)	Yb (ppm)	Lu (ppm)	Pb (ppm)	Th (ppm)	U (ppm)	A/CNK	A/NK
A1-1	0.71	2.06	0.30	1.95	0.30	18.1	9.66	2.44	0.92	1.69
A2-7-5	0.34	0.93	0.14	0.94	0.15	8.06	7.25	1.59	1.12	1.38
A2-6	0.29	0.75	0.11	0.71	0.11	8.68	4.99	3.45	1.06	1.60
EK-1	0.33	1.01	0.17	1.21	0.20	26.0	18.3	1.96	1.01	1.11
Zh-2–10	0.52	1.73	0.31	2.44	0.46	21.5	14.2	19.1	0.98	1.15
S1-1	0.40	1.09	0.15	0.95	0.15	7.36	8.17	1.99	0.88	1.47
Ash-1	0.54	1.52	0.24	1.61	0.26	16.8	27.8	8.68	0.96	1.46
Ak-3	0.81	2.23	0.34	2.13	0.34	14.8	9.91	2.61	0.88	1.95

3.3 Sayak-I Skarn Cu deposit and Akzhal Pb-Zn deposit

The Sayak-I skarn Cu deposit, as the largest deposit in the Sayak skarn ore district, is located within the Sayak basin which is filled with marine volcanogenic rocks, carbonate and terrigenous molasses sediments of Middle Visean–Middle Carboniferous age (Fig. 1). The proven Cu reserves of the deposits are 1 Mt, with grades of 1.14–3.21% Cu (Kudryavtsev, 1996). The Sayak-I skarn Cu deposit is in the western exocontact of the Lebai granodiorite pluton (S1-1), and occurs in carbonate rocks located within an anticlinal bend. The width of near-intrusion skarn zones range from 500 to 1000 m and the total length is about 3 km. In immediate contact with granodiorite pluton, limestone is completely transformed into skarn. The granodiorite (S1-1) has SIMS zircon concordia age of 311.4 ± 2.5 Ma (our unpublished data). S1-1 belongs to I-type series and has metaluminous features, with magnetite as the main opaque mineral.

The Akzhal Pb-Zn deposit lies 20 km south of the Akshatau W-Mo deposit (Fig. 1). The orebody is emplaced into the Akzhal-Aksaran syncline composed of Late Devonian Brakhiskladok Formation, which consists of silicic carbonatite and calcic terrigenous clastic rocks. In the west part of the deposit, diorite-porphyry (Ak-3) intruded into the Akzhal-Aksaran syncline and caused skarn alteration. In this deposit, 85% of Pb-Zn reserves are located in the skarn, and the deposit is represented by disseminated, veinlet-disseminated and massive orebodies. The Akzhal Pb-Zn deposit has average grades of 1.14% of Pb, and 4.87% of Zn. The age of the diorite porphyry and ore formation is unknown. The values of A/CNK and A/NK for Ak-3 are 0.88 and 1.95, which suggest Ak-3 as metaluminous and of I-type

character. The major opaque minerals are magnetite, less pyrite and chalcopyrite.

4. Petrographic details concerning apatite occurrence

Details of 12 plutons such as sample location, lithology, mineral assemblage and accessory mineral phases are listed in Table 1. Apatite occurrence in representative rocks will be described in detail as follows.

In the granodiorite (A1-1) at the Aktogai porphyry Cu-Mo deposit, apatite occurs mainly with biotite, hornblende and magnetite as included phases in these minerals or associated phases along these minerals (Fig. 2a). Subhedral and euhedral apatite in A1-1 ranges from 24.3 to 243 μm. In the representative porphyries (A2-2, A2-6,

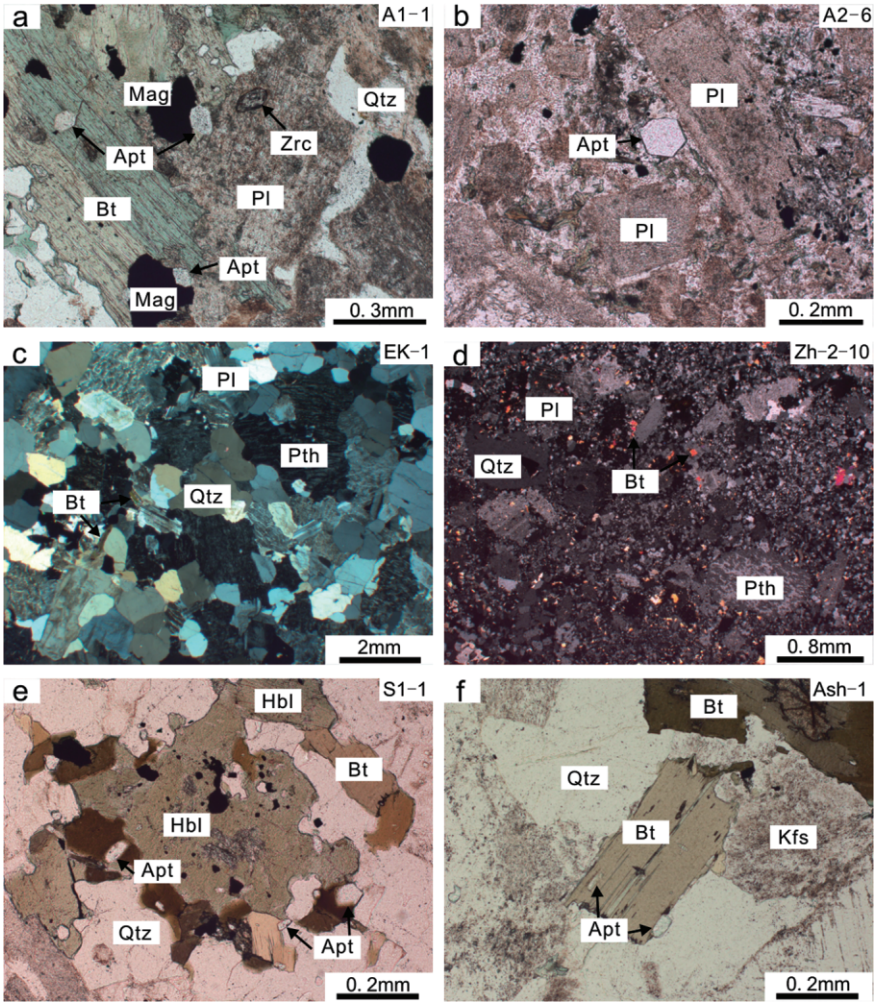

Fig. 2 Photomicrographs showing the mineral assemblages and the occurrence of apatite in plutons from Central Kazakhstan. (a) Apatites occur with hornblende and magnetite as included phases in these minerals or associated phases along these minerals in sample A1-1 granodiorite from the Aktogai porphyry Cu-Mo deposit, open-nicol. (b) Euhedral hexagon phenocrysts apatite locates in the matrix between plagioclase phenocrysts in sample A2-6 granodiorite porphyry from Aktogai porphyry Cu-Mo deposit, open-nicol. (c) The assemblage of perthite, quartz, plagioclase and biotite in EK-1 syenogranite from the East Kounrad Mo-W deposit, crossed-nicol. (d) The phenocrysts of perthite, plagioclase and quartz in Zh-2–10 syenogranite porphyry from the Zhanet Mo-W deposit, crossed-nicol. (e) Euhedral or subhedral apatites occur with biotite and hornblende as included phases in these minerals in S1-1 granodiorite from the Sayak-I skarn Cu deposit, open-nicol. (f) Euhedral apatites locate along the biotite boundary or along the cleavage of biotite in Ash-1 granite from the Akshatau W-Mo deposit, open-nicol. Apt: Apatite, Bt: Biotite, Hbl: Hornblende, Kfs: K-feldspar, Mag: Magnetite, Pth: Perthite, Pl: Plagioclase, Qtz: Quartz, Zrc: Zircon.

A2-7-1) at Aktogai, apatite occurs as mineral inclusions and groundmass intergranular apatite. Inclusion apatite is subhedral to euhedral, ranging from 7.7 to 299 μm in size. These apatites are included in biotite, feldspar and magnetite, more rarely hornblende, and therefore precipitated earlier than the host minerals. Relatively coarse-grained subhedral to euhedral groundmass intergranular apatite ranges from 40 to 300 μm. The matrix intergranular apatite shows more euhedral than inclusion apatite. Rarely euhedral hexagon phenocryst of apatite is observed in A2-6 (Fig. 2b).

In the syenogranite (EK-1, Fig. 2c) at East Kounrad, apatite occurs primarily as inclusions phase of biotite, more rarely magnetite, and occasionally as intergranular crystals. Grain size and morphology are highly variable. Apatite is randomly oriented in the biotite. According to the apatite occurrence, apatite precipitated earlier than or later than biotite.

In the granodiorite (S1-1) at the Sayak-I skarn Cu deposit, apatite mainly occurs with biotite and hornblende, rarely magnetite, as mineral inclusions or associated phases along these minerals (Fig. 2e). Subhedral and euhedral apatite in S1-1 ranges from 13.0 to 183 μm. Larger apatite crystals are included in hornblende more than biotite. This occurrence suggests hornblende crystallized earlier than biotite, which is also supported by the observation that biotite grows around hornblende.

In the granite (Ash-1) at Akshatau, nearly all biotites contain euhedral or subhedral apatite, many of which are aligned parallel to the cleavage in biotite, or along the biotite boundary (Fig. 2f), while others lie in or along magnetite. Grain size and morphology are highly variable, ranging from euhedral to subhedral grains between 16.4 and 242 μm.

In the diorite porphyry (Ak-3) at Akzhal, apatite occurs primarily as an inclusion within hornblende, biotite and magnetite, and as groundmass intergranular grains. The grain size of apatite is independent of its mode of occurrence (included or intergranular grains), and ranges from 25.7 to 142 μm.

Zoning apatite in back-scattered electron images (BSE) has not been observed in any sample. Fine-grained mineral inclusions are observed in apatite, such that the A2-3-2 apatites containing anhydrite, and those of Ek-1 and Zh-2–10 containing fluorite.

5. Analytical methods

Heavy-mineral separation methods have been used to obtain apatite concentrates. Apatite grains with no visible inclusions were picked out under binocular microscope, mounted in epoxy blocks and then polished. Polished sections were carbon-coated for electron microprobe analysis.

Major- and minor-element compositions of apatite were measured at the Institute of Geology and Geophysics, Chinese Academy of Sciences (IGGCAS), using a JEOL-JXA8100 electron microprobe operated in wavelength-dispersive spectrometers (WDS). The operating conditions were 15 kV accelerating voltage and 10 nA beam current. Twenty seconds (s) of counting time were chosen for most elements, except 40 s for F, and 10 s for P and Ca at their characteristic X-rays. Natural minerals and synthetic oxides were used as standards, and all data were corrected based on the ZAF procedure (Henoc & Tong, 1978). Ca was used as the internal standard for trace-element determinations by LA-ICP-MS.

Trace-element contents of apatites were determined in the LA-ICP-MS apparatus at the State Key Laboratory of Geological Processes and Mineral Resources, China University of Geosciences (Wuhan). Detailed operating conditions for laser ablation system and ICP-MS in structure are the same as those described by Liu *et al*. (2008). Laser sampling was performed on a Geolas 2005. Ion-signal intensities were acquired through an Agilent 7500a ICP-MS instrument with helium (He) as the carrier gas and argon (Ar) as make-up gas. He and Ar were mixed via a T-connector before entering the ICP. Nitrogen (N_2) was added into the central He-Ar gas flow of the Ar plasma, in order to lower the detection limit and improve precision (Hu *et al*., 2008). Spot sizes of 44 μm and 60 μm were chosen in this study. Each analysis incorporated a background acquisition for approximately 20–30 s (gas blank) followed by 50 s of data acquisition.

Ca content in apatite obtained from EMPA was used as internal standard to correct matrix effects, signal drift and differences in the ablation yield between samples and reference materials in ICP-MS. The external standards used for the apatite in situ analysis are NIST SRM 610, BCR-2G, BIR-1G and BHVO-2G. The preferred values of element concentrations for the USGS reference glasses are from Norman *et al*. 1996, 1998) and the GeoReM database (http://georem.mpch-mainz.gwdg.de/). Off-line selection, integration of background and analysis signals, time-drift correction and quantitative calibration were performed by ICPMSDataCal (Liu *et al*., 2008, 2010). The LA-ICPMS data agree well with the recommended values of the standards, and precision is higher than

5% for most of the 20 elements. Representative chemical compositions of the apatites are shown in Table 3.

6. Results

6.1 Apatite major elements

The analytical results show that CaO and P_2O_5, both principal components of apatite, exhibit few variations, most ranging from 53.0 to 56.5 wt% for CaO and from 40.5 to 44.0 wt% for P_2O_5, respectively. Al_2O_3 contents are typically lower than 0.10 wt% without systematic variation, and the concentrations of Ti, Ba and K rarely exceed 0.06, 0.07 and 0.03 wt%, respectively.

6.1.1 Fluorine and chlorine

All the apatites are fluorapatites, which is typical for igneous origin (Nash, 1984). In general, the content of Cl in apatites negatively correlates with that of F (Fig. 3a). In particular, a broad range of content for Cl in apatites from A1-1 (Aktogai) and Ak-3 (Akzhal) is observed. Ak-3 apatite from the Akzhal Pb-Zn deposit shows the lowest F/Cl ratio and the highest Cl concentration. In contrast, apatites from Aktogai porphyries, Sayak granodiorite and Akshatau granite have relatively uniform Cl and F contents, ranging from the content below the detection limit (bdl) to 0.80 wt% for Cl, and from 2.10 to 4.00 wt% for F, respectively. However, a higher F content (typically > 3.6 wt%) but with trace Cl content, thus higher F/Cl ratio, appears in apatites of Ek-1 (East Kounrad), Zh-2–10 (Zhanet) and Zh-2–1 (Zhanet) from the Mo-W deposits (Fig. 3b), which is consistent with the observed abundant primary fluorite in apatite.

6.1.2 Sodium, sulfur and silicon

The apatites in A1-1 (Aktogai) are characterized by low and constant Na_2O (<0.20 wt%) and SO_3 (<0.10 wt%) concentrations with one exception. However, there is a large overlap on Na_2O-SO_3 contents for apatite from Aktogai porphyries, Sayak and Akshatau granitoids (bdl–0.20 wt% for Na_2O and bdl–0.28 wt% for SO_3). Nevertheless, Na_2O-SO_3 contents of apatite in Ek-1 (East Kounrad), Zh-2–1 (Zhanet), Zh-2–10 (Zhanet) and Ak-3 (Akzhal) are widely spread (0.10–0.55 wt% for Na_2O, and 0.10–0.55 wt% for SO_3). Obvious positive correlation of Na_2O and SO_3 in apatites is displayed in Figure 3c, which probably indicates the coupled substitution of $S^{6+}+Na^{+} = Ca^{2+}+P^{5+}$ in apatites (Sha & Chappell, 1999).

6.1.3 Manganese, iron and magnesium

Distinct contents of MnO, FeO and MgO in apatites for different types of deposits are obvious (Table 4). Most of the apatites from A1-1, S1-1 and Ak-1 contain few MnO (<0.10 wt%), and MgO (<0.07 wt%), and with variable content of FeO (<0.28 wt%, <0.15 wt% and <0.42 wt%, respectively). However, apatites of Aktogai porphyries (A2-2, A2-3-2, A2-7-1, A2-7-5 and A2-6) show high contents of MnO (0.08–0.28 wt%), FeO (0.13–0.36 wt%) and MgO (0.03–0.15 wt%). Meanwhile, apatites of Ek-1 (East Kounrad), Zh-2–1 (Zhanet) and Zh-2–10 (Zhanet) display high MnO (typically >0.20 wt%), low MgO (<0.04 wt%) but variable FeO (ranging from bdl to 0.25 wt%). A positive correlation between whole-rock SiO_2 and apatite MnO indicates that MnO content in apatite may be mainly related with the degree of magmatic differentiation (Fig. 3d) (Belousova *et al*., 2001; 2002).

6.2 Apatite trace elements

6.2.1 Uranium, thorium and lead

No obvious differences for Th (7.60–101 ppm) and Pb (1.50–17.1 ppm) abundances among apatites are identified for different types of deposits (Table 4). Apatites of A2-2 (Aktogai), A2-3-2 (Aktogai), A2-7-1 (Aktogai), S1-1 (Sayak-I) and Ash-1 (Akshatau) show higher U contents with mean values ranging from 32.7 to 40.4 ppm, while apatites of other samples exhibit lower contents of U (mean 4.40–8.80 ppm). The low Th/U ratio is likely due to higher contents of U, as for other samples with low abundance of U, high Th/U ratio is found (Fig. 4a).

6.2.2 Vanadium

Compared with other samples (V content of 5.00–30.0 ppm), obvious higher contents of V in apatites from S1-1 (Sayak-I), A1-1 (Aktogai) and Ak-3 (Akzhal) are detected, with mean values of 36.2 ppm, 27.3 ppm (two samples) and 19.9 ppm, respectively (Table 4). Higher V abundances may not be attributed to the degrees of oxidation but the high contents of V in host granitic rocks (Table 2), despite that V can enter apatite in the form of VO_4^{3-} which substitutes PO_4^{3-} in apatite without any coupled substitution (Bhatnagar, 1969; Kutoglu, 1974; Wilson *et al*., 1977), as the three samples above do not have the most oxidative state.

6.2.3 Strontium and yttrium

A widespread distribution of the contents of Sr (50.0–1000 ppm) and Y (from 184 ppm to several thousand

Table 3 Mean major- and trace-element composition of apatites from Central Kazakhstan (bdl: below detection limits)

Sample	A1-1				A2-2				A2-3-2				A2-7-1				A2-7-5				A2-6			
	Mean	Max.	Min.	1σ	Mean	Max.	Min.	1σ	Mean	Max.	Min.	1σ	Mean	Max.	Min.	1σ	Mean	Max.	Min.	1σ	Mean	Max.	Min.	1σ
Major element (wt%)																								
P_2O_5	42.0	42.9	40.9	0.58	42.0	43.2	40.2	0.64	42.5	43.3	41.7	0.45	42.5	43.8	41.0	0.67	42.1	43.0	40.7	0.60	42.6	43.7	41.1	0.60
CaO	55.0	56.7	53.4	0.83	55.1	56.0	54.2	0.44	54.3	55.9	53.3	0.51	54.9	55.5	53.6	0.47	55.0	56.5	54.2	0.48	55.3	56.3	54.7	0.33
SiO_2	0.17	0.38	0.04	0.10	0.05	0.19	0.03	0.05	0.07	0.19	bdl	0.06	0.06	0.33	bdl	0.08	0.06	0.14	bdl	0.05	0.11	0.21	bdl	0.05
Al_2O_3	0.07	0.51	0.02	0.12	0.03	0.14	0.02	0.03	0.04	0.16	bdl	0.04	0.05	0.36	bdl	0.10	0.01	0.04	bdl	0.01	bdl			
FeO	0.09	0.33	0.06	0.10	0.26	0.36	0.15	0.05	0.23	0.42	bdl	0.08	0.19	0.29	0.07	0.06	0.23	0.32	0.15	0.05	0.24	0.36	0.13	0.05
MnO	0.04	0.12	0.06	0.04	0.17	0.28	0.08	0.05	0.19	0.28	0.09	0.04	0.23	0.29	0.14	0.04	0.19	0.29	0.09	0.05	0.19	0.27	0.11	0.04
MgO	0.02	0.08	0.02	0.03	0.08	0.13	0.04	0.02	0.08	0.13	0.04	0.02	0.10	0.13	0.03	0.03	0.09	0.14	0.03	0.03	0.05	0.07	bdl	0.02
Na_2O	0.08	0.20	0.02	0.06	0.13	0.26	0.07	0.04	0.12	0.20	0.07	0.04	0.13	0.38	0.05	0.07	0.14	0.20	0.07	0.03	0.12	0.20	0.06	0.03
K_2O	bdl				bdl				bdl				bdl				bdl				bdl			
TiO_2	bdl				bdl				bdl				bdl				bdl				bdl			
BaO	bdl				bdl				bdl				bdl				bdl				bdl			
Cl	0.71	1.77	0.09	0.57	0.30	0.41	0.14	0.07	0.33	0.49	0.11	0.10	0.33	0.39	0.23	0.05	0.33	0.45	0.19	0.08	0.50	0.76	0.22	0.12
F	2.94	3.56	2.39	0.36	3.33	3.91	3.01	0.24	3.16	4.23	2.76	0.30	3.35	5.15	2.85	0.54	3.20	3.61	1.89	0.34	2.99	3.35	2.61	0.19
SO_3	0.05	0.71	bdl	0.14	0.10	0.33	bdl	0.07	0.09	0.27		0.06	0.08	0.29	bdl	0.06	0.09	0.13	0.04	0.02	0.19	0.38	0.09	0.07
F,Cl = –O	1.40	1.52	1.33	0.05	1.47	1.71	1.35	0.10	1.41	1.82	1.24	0.12	1.48	2.24	1.28	0.23	1.42	1.56	0.86	0.15	1.37	1.53	1.27	0.07
No. of grains	27				32				33				16				29				32			
Trace element (ppm)																								
V	27.3	39.2	15.4	16.8	15.6	33.5	1.22	11.0	10.7	19.1	4.4	4.70	7.21	10.4	2.61	2.69					17.4	30.7	3.99	7.95
Sr	227	238	217	14.9	500	827	406	129	421	432	395	8.56	455	495	421	26.9					590	681	539	42.2
Th	19.9	23.4	16.5	4.85	39.7	96.4	13.2	25.8	27.9	41.3	8.66	9.48	34.0	66.9	19.6	17.0					25.2	37.0	10.47	8.06
U	4.19	4.26	4.11	0.10	32.1	49.6	5.83	13.4	30.9	49.1	9.66	12.0	38.6	50.7	23.6	10.5					39.7	66.1	14.0	15.7
Pb	3.78	4.18	3.37	0.57	3.51	4.71	2.65	0.73	3.18	5.08	2.28	0.66	4.04	4.42	3.59	0.33					3.93	5.56	2.72	0.70
La	990	1176	804	263	580	1240	149	322	495	1209	174	216	470	801	281	196					737	1057	296	237
Ce	2530	2936	2124	574	1659	2762	604	701	1441	2840	609	478	1387	1927	881	407					1499	1984	629	404
Pr	358	407	308	69.9	267	400	124	94.8	218	351	131	50.0	217	270	163	39.8					173	231	66.6	46.1
Nd	1595	1792	1398	278	1257	1885	697	397	1180	1534	764	232	1143	1425	898	195					730	1028	273	207
Sm	356	388	323	46.1	330	460	173	96.9	324	393	236	51.9	316	376	254	51.9					120	188	49.3	41.7
Eu	8.77	8.9	8.6	0.23	40.9	48.8	31.0	4.98	47.2	54.6	39.3	4.99	39.0	43.2	33.2	3.08					27.4	42.2	14.3	8.25
Gd	340	363	316	33.6	308	389	118	87.9	307	372	232	38.7	307	368	242	48.9					93.2	158	44.1	34.7
Tb	44.9	47.6	42.2	3.81	48.0	63.8	13.4	14.7	48.2	58.7	37.6	5.15	48.2	56.2	39.0	6.99					11.7	22.5	5.47	5.25
Dy	246	261	232	20.7	295	408	66	95.1	276	339	219	30	283	334	229	37.5					65.4	137	31.3	32.4
Ho	47.0	49.5	44.5	3.52	60.5	87.0	12.1	20.2	60.6	75.0	46.5	6.98	62.6	73.6	51.27	7.38					12.6	27.2	5.90	6.48
Er	116	122	110	8.86	175	258	31	60.4	168	211	123	22.0	168	202	137	19.7					33.2	75.2	16.0	17.8
Tm	14.2	14.7	13.7	0.74	27.7	41.1	4.32	9.82	25.2	33.3	17.5	3.83	26.5	32.2	21.30	3.36					4.81	11.4	2.12	2.74
Yb	71.5	74.6	68.5	4.28	179	267	24	65.4	161	218	106	26.8	167	204	132	23.8					33.5	81.4	13.9	19.2
Lu	8.87	9.23	8.52	0.50	24.6	37.3	3.35	9.09	24.7	33.6	16.4	4.21	26.6	32.7	21.1	3.94					4.83	11.8	2.05	2.74
Y	1304	1376	1231	102	1597	2291	334	523	1448	1768	1198	143	1498	1741	1205	182					470	776	184	182
No. of grains	2				10				20				7								17			

Table 3 Continued

Sample	Ek-1				Zh-2–1				Zh-2–10				S1-1				Ash-1				Ak-3			
	Mean	Max.	Min.	1σ	Mean	Max.	Min.	1σ	Mean	Max.	Min.	1σ	Mean	Max.	Min.	1σ	Mean	Max.	Min.	1σ	Mean	Max.	Min.	1σ
Major element (wt%)																								
P_2O_5	41.5	42.5	39.9	0.53	42.2	43.3	41.5	0.46	42.5	43.2	41.5	0.48	42.3	43.0	41.0	0.46	42.8	43.7	41.5	0.49	42.1	43.4	40.9	0.49
CaO	54.3	55.2	53.1	0.57	54.5	55.2	53.6	0.52	54.1	55.2	52.4	0.65	55.1	56.1	53.9	0.56	55.7	56.5	55.0	0.35	55.3	56.6	54.1	0.55
SiO_2	0.34	0.73	0.23	0.10	0.26	0.49	0.07	0.14	0.17	0.39	bdl	0.12	0.20	0.37	bdl	0.07	0.19	0.49	0.07	0.09	0.17	0.29		0.08
Al_2O_3	bdl	0.15	bdl		0.01	0.03	bdl	0.01	0.04	0.34	bdl	0.08	bdl	0.27	bdl		bdl	0.06	bdl		0.02	0.07		0.02
FeO	bdl	0.09	bdl		0.15	0.24	bdl	0.08	0.10	0.21	bdl	0.05	bdl	0.14	bdl		bdl	0.09	bdl		0.18	0.42		0.13
MnO	0.28	0.44	0.20	0.06	0.32	0.49	0.18	0.10	0.27	0.46	0.18	0.07	bdl	0.10	bdl		0.14	0.25	bdl	0.06	bdl	0.12		0.04
MgO		0.04	bdl	0.01	0.01	0.03	bdl	0.01	0.01	0.04	bdl	0.01	bdl	0.06	bdl		bdl	0.04	bdl		0.14	0.28		0.11
Na_2O	0.22	0.44	0.09	0.09	0.21	0.34	0.14	0.06	0.28	0.54	0.14	0.08	0.13	0.25	0.02	0.06	0.07	0.18	0.03	0.04	0.15	0.27	0.02	0.07
K_2O	bdl				bdl				bdl				bdl				bdl				bdl			
TiO_2	bdl				bdl				bdl				bdl				bdl				bdl			
BaO	bdl				bdl				bdl				bdl				bdl				bdl			
Cl				0.01	0.05	0.26	0.02	0.07	0.03	0.08	bdl	0.02	0.55	0.83	0.07	0.19	0.35	0.52	0.08	0.10	1.05	2.34	0.11	0.47
F	3.82	4.23	3.66	0.12	4.17	5.05	3.88	0.38	4.23	5.15	3.62	0.36	2.60	3.46	2.14	0.32	3.02	3.70	2.67	0.23	2.74	3.71	1.68	0.54
SO_3	0.36	0.73	0.16	0.19	0.21	0.58	0.05	0.17	0.21	0.53	0.06	0.13	0.15	0.36	0.03	0.09	0.14	0.53	0.04	0.09	0.26	0.55	bdl	0.18
F,Cl = –O	1.61	1.78	1.54	0.05	1.77	2.14	1.64	0.16	1.79	2.17	1.53	0.15	1.22	1.54	1.06	0.11	1.35	1.58	1.23	0.08	1.39	1.75	0.97	0.18
No. of grains	33				10				28				37				30				31			
Trace element (ppm)																								
V	15.3	32.3	4.06	8.00					9.22	24.1	0.71	5.10	38.0	68.5	22.9	10.9	16.1	65.9	7.92	13.4	19.9	30.2	5.31	8.41
Sr	158	281	38.2	67.7					227	280	200	18.5	577	710	432	84.6	147	173	117	18.5	765	960	343	223
Th	31.4	97.8	14.7	18.3					39.3	76.7	17.5	18.2	65.1	101	25.8	20.1	39.7	75.8	19.0	13.6	20.5	44.2	7.60	8.52
U	5.03	11.3	3.01	1.94					8.78	18.7	2.63	3.83	33.1	61.7	10.2	12.1	40.4	74.2	17.7	14.8	4.17	8.29	0.83	1.81
Pb	8.52	12.7	6.46	1.66					8.61	13.4	5.87	1.84	4.11	6.69	1.98	1.26	4.61	7.42	3.31	1.07	4.11	17.1	1.54	3.14
La	2457	3689	1635	514					1659	2381	1147	309	1891	2542	1194	393	773	1495	560	219	521	1110	197	201
Ce	4990	7270	3439	860					4479	6671	3439	836	3854	4978	2616	715	1693	2819	1078	433	1220	2379	604	393
Pr	504	675	309	87.4					620	867	474	106	416	516	310	67.9	195	302	115	51.0	160	285	94.6	44.1
Nd	1795	2362	1159	285					2531	3188	1863	378	1569	1917	1220	234	818	1328	456	223	731	1205	511	178
Sm	332	643	153	121					683	909	465	115	210	254	167	28.3	147	244	77.4	43.1	145	209	99.1	32.5
Eu	31.0	40.9	13.7	6.26					48.2	61.7	34.6	8.85	15.2	19.6	9.3	3.05	10.5	21.7	5.40	3.62	21.7	31.8	5.91	7.76
Gd	314	757	133	151					745	1029	501	137	149	188	119	20.3	145	226	78.1	40.1	135	203	88.6	31.2
Tb	50.5	153	17.3	33.3					138	196	93.4	28.7	16.4	21.2	12.9	2.43	18.8	28.4	10.0	5.38	17.2	26.1	10.8	4.05
Dy	277	830	89.5	189					921	1323	632	199	83.2	108	63.8	13.1	108	160	58.7	30.9	92.8	142	56.3	22.3
Ho	64.4	193	19.9	46.5					196	281	135	43.4	15.4	20.7	11.9	2.47	22.7	32.8	13.1	6.35	17.1	25.7	10.4	4.10
Er	188	571	55.5	140					583	812	409	131	37.9	53.8	28.5	6.55	60.9	89.8	35.7	17.2	40.1	59.8	24.7	9.43
Tm	28.8	93.4	8.06	22.9					97.3	143	67.3	22.9	4.79	7.34	3.54	0.91	8.30	12.9	4.56	2.41	4.79	6.92	2.93	1.08
Yb	189	620	51.6	153					641	980	429	158	28.8	46.2	21.0	5.74	55.4	89.2	30.2	16.3	27.3	38.3	17.4	5.91
Lu	30.1	98.3	8.73	24.1					87.7	143	58.3	23.2	4.11	6.87	2.94	0.86	9.50	14.7	5.28	2.69	3.59	4.93	2.31	0.73
Y	2298	7313	650	1803					3896	5511	2920	713	415	616	323	64.5	717	1016	427	200	482	705	283	116
No. of grains	21								19				23				19				21			

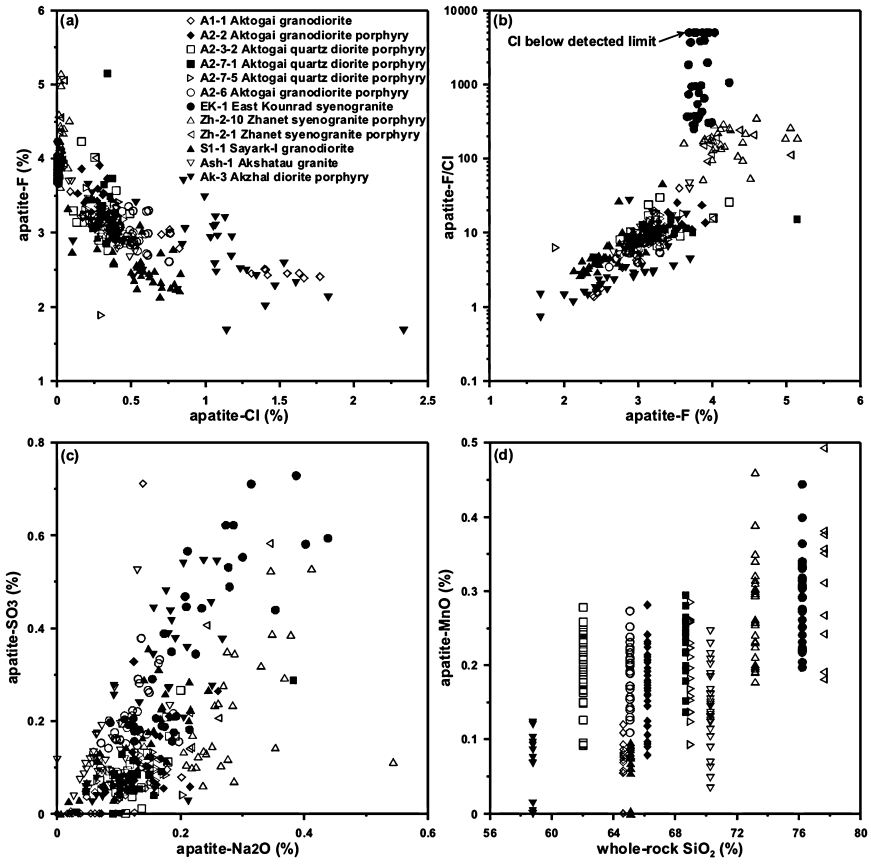

Fig. 3 Minor element composition of apatites from different ore deposits: (a) apatite-F versus apatite-Cl; (b) apatite-F/Cl versus apatite-F; (c) apatite-SO_3 versus apatite-Na_2O; (d) apatite-MnO versus whole-rock SiO_2.

ppm) is observed in apatites from different deposits. Obvious different correlations for Sr and Y in apatites with whole-rock SiO_2 suggest that the content of Sr decrease, while Y increases during the magmatic differentiation process (Fig. 4b, c). Most samples have limited Sr and Y abundances, for example, A2-2 (Aktogai), A2-3-2 (Aktogai) and A2-7-1 (Aktogai) have the same concentrations of Sr (395–827 ppm) and Y (1198–1824 ppm) (Fig. 4d).

6.2.4 Rare earth element

Higher light REE (LREE) (La-Eu) and total REE+Y are enriched in apatites in the two Mo-W deposits, Zh-2–10 (Zhanet) and EK-1 (East Kounrad) comparing with other samples (Fig. 4e). Apatites in A2-2 (Aktogai), A2-3-2 (Aktogai), A2-7-1 (Aktogai) and Zh-2–10 (Zhanet) exhibit the lowest $(La/Yb)_N$ and $(La/Sm)_N$ ratios, while apatites of S1-1 (Sayak-I) display the highest $(La/Yb)_N$ (mean value of 44.7) and $(La/Sm)_N$ (mean value of 5.64) (Fig. 4f, Table 4).

Apatites in A2-6 (Aktogai) contain the weakest negative $(Eu/Eu^*)_N$ (0.51–0.99), except two points with values of more than 1. Other apatites display relatively moderate negative $(Eu/Eu^*)_N$, ranging from 0.21 to 0.48, except sample Aktogai A1-1, which has the strongest negative $(Eu/Eu^*)_N$ values of 0.072–0.081 (Table 4). Ce content higher than 2000 ppm is detected in apatites of S1-1 (Sayak-I), EK-1 (East Kounrad) and Zh-2–10 (Zhanet).

Apatites from different types of deposits show significant variations in chondrite-normalized REE patterns (Fig. 5). According to chondrite-normalized REE patterns, apatites are divided into four types: type 1, A1-1 (Aktogai), S1-1 (Sayak-I) and Ak-3 (Akzhal), distinguished by right-inclined REE pattern with largest $(La/Yb)_N$ ratio, and strong negative $(Eu/Eu^*)_N$; type 2, A2-2 (Aktogai), A2-3-2 (Aktogai) and A2-7-1 (Aktogai), characterized by weekly right-inclined REE pattern with upward-convex LREE, and relatively strong negative $(Eu/Eu^*)_N$; type 3, EK-1 (East Kounrad) and

Table 4 Summary of characteristic features of minor and trace elements in apatites from different types of deposits of Central Kazakhstan

Sample	A1-1	A2-2, A2-3-2, A2-7-1	A2-6	EK-1	Zh-2–1, Zh-2–10	S1-1	Ash-1	Ak-3
F (%)	2.39–3.56, mean 2.94	1.89–5.15, mean 3.25	2.61–3.35, mean 2.99	3.66–4.23, mean 3.82	3.62–5.15, mean 4.22	2.14–3.46, mean 2.60	2.67–3.70, mean 3.02	1.68–3.71, mean 2.74
Cl(%)	0.09–1.77	<0.50, mean 0.32	0.22–0.76, mean 0.50	<0.10	<0.10	0.07–0.83, mean 0.55	0.08–0.52, mean 0.35	0.11–2.34, mean 1.05
F/Cl	1.40–40.0, mean 9.00	6.20–29.9, mean 11.1	3.50–14.6, mean 6.40	mostly >300	100–300, mean 175	2.70–46.3, mean 6.80	5.20–46.7, mean 11.0	0.70–26.9, mean 4.30
SO_3 (%)	mostly <0.10	0–0.33, mean 0.09	0.09–0.38, mean 0.19	0.16–0.73, mean 0.36	0.05–0.58, mean 0.21	0–0.36, mean 0.15	0.04–0.27, mean 0.14	0–0.55, mean 0.26
Na_2O(%)	0–0.20, mean 0.08	0.05–0.24, mean 0.13	0.06–0.20, mean 0.12	0.09–0.44, mean 0.22	0.14–0.54, mean 0.26	0–0.25, mean 0.13	0–0.18, mean 0.07	0.02–0.27, mean 0.15
SiO_2(%)	0–0.38, mean 0.17	0–0.21, mean 0.11	0–0.21, mean 0.11	0.23–0.57, mean 0.34, with exception 0.73	0–0.49, mean 0.20	0–0.37, mean 0.20	0.07–0.49, mean 0.19	0–0.29, mean 0.17
Al_2O_3(%)	0–0.51, mean 0.07	mostly <0.10	mostly <0.10	mostly <0.10	mostly <0.10	mostly <0.15	<0.06	<0.07
FeO(%)	0–0.33, mean 0.09	0.13–0.42, mean 0.23	0.13–0.36, mean 0.24	<0.10	0–0.24, mean 0.11	mostly <0.10	<0.10	0–0.42, mean 0.18
MnO(%)	<0.12	0.08–0.29, mean 0.19	0.11–0.27, mean 0.19	0.20–0.44, mean 0.28	0.18–0.49, mean 0.28	<0.10	0–0.25, mean 0.14	<0.12
MgO(%)	<0.07	0.03–0.14, mean 0.09	<0.07	<0.05	<0.05	<0.05	<0.04	0–0.28, mean 0.14
V (ppm)	15.4–39.2	1.2–33.5, mean 11.4	4.00–30.7, mean 16.6	4.10–32.3, mean 15.3	0.70–24.1, mean 9.20	15.1–68.5, mean 36.2	7.90–65.9, mean 15.7	5.30–30.2, mean 19.9
Sr (ppm)	217–238	395–827, mean 449	539–681, mean 592	38.2–281, mean 158	200–280, mean 227	432–710, mean 579	117–173, mean 146	343–960, mean 765
Th (ppm)	16.5–23.4	8.70–96.4, mean 32.3	10.5–45.0, mean 28.7	14.7–97.8, mean 31.4	17.5–76.7, mean 39.3	mostly 25.8–101, mean 65.1	19.0–82.2, mean 41.8	7.60–44.2, mean 20.5
U (ppm)	4.11–4.26	5.80–50.7, mean 32.7	mostly 14.0–66.1, mean 39.7	3.00–11.3, mean 5.00	2.30–18.7, mean 8.80	10.2–61.7, mean 33.1	17.7–74.2, mean 40.4	0.80–8.30, mean 4.20
Pb (ppm)	3.37–4.18	2.30–5.10, mean 3.40	2.70–5.60, mean 4.10	6.50–12.7, mean 8.50	5.90–13.4, mean 8.60	2.00–6.90, mean 4.30	3.30–7.60, mean 4.80	1.50–17.1, mean 4.10
Y (ppm)	1231–1376	1198–1824, mean 1508	184–925, mean 470	650–7313, mean 2298	2920–5511, mean 3896	323–658, mean 432	427–1016, mean 717	283–705, mean 482
Th/U	3.88–5.68	0.35–3.87, mean 1.12	0.32–1.47, mean 0.62	4.60–8.60, mean 6.00	2.70–7.60, mean 4.60	1.20–3.80, mean 2.10	0.50–2.6, mean 1.10	3.70–14.0, mean 5.90
$(Eu/Eu^*)_N$	0.072–0.081	0.30–0.63, mean 0.43	0.51–1.18, mean 0.80	0.12–0.47, mean 0.32	0.15–0.25, mean 0.21	0.18–0.30, mean 0.25	0.13–0.42, mean 0.23	0.13–0.64, mean 0.48,
LREE/HREE	5.95–7.12	2.00–16.3, mean 3.80	5.00–22.6, mean 12.5	3.10–18.4, mean 11.4	2.30–4.00, mean 3.00	13.2–27.3, mean 23.4	6.50–12.8, mean 8.70	4.40–11.9, mean 8.40
$(La/Yb)_N$	7.93–10.7	0.72–4.10, mean 1.89	3.49–41.3, mean 19.9	2.07–27.1, mean 13.69	1.37–2.76, mean 1.80	17.5–53.6, mean 44.7	5.98–17.3, mean 9.94	4.91–22.2, mean 13.0
REE pattern	Similar to S1-1, but with the strongest negative Eu/Eu*	LREE weekly enriched with some upward-convexed, flattened on both MREE and HREE	Similar to Ash-1, but with weekly negative Eu/Eu*	LREE-enriched, strong negative Eu/Eu*, flattened on both MREE and HREE, Nd depletion	similar to EK-1, but with less LREE enrichment to HREE	right-inclined, with largest $(La/Yb)_N$, and strong negative Eu/Eu*	LREE-enriched, strong negative Eu/Eu*, flattened on HREE	Similar to S1-1

LREE, light REE; HREE, heavy REE; MREE, middle REE.

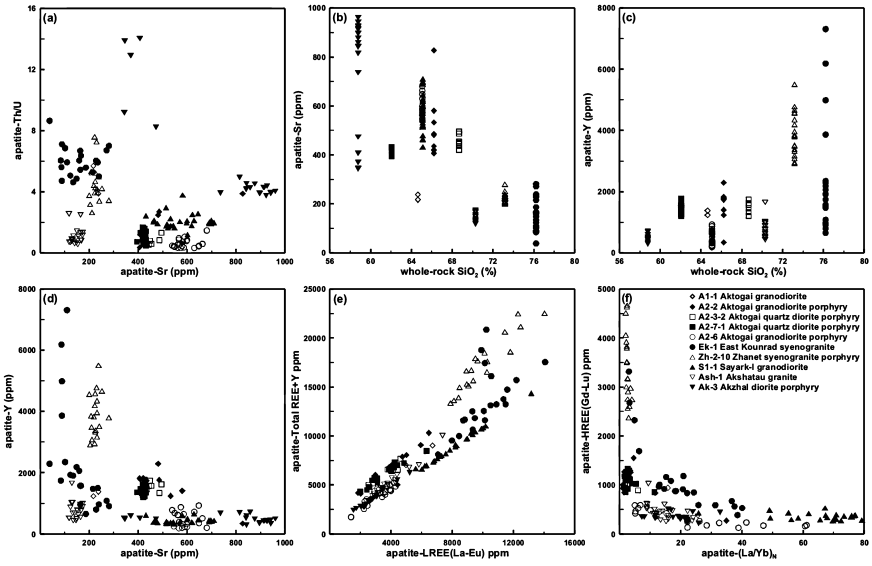

Fig. 4 Variation of (a) Th/U versus Sr (b) Sr versus SiO_2 (c) Y versus SiO_2 (d) Y versus Sr (e) Total REE and Y versus light REE (LREE) (f) heavy REE (HREE) versus $(La/Yb)_N$ in apatites from different ore deposits.

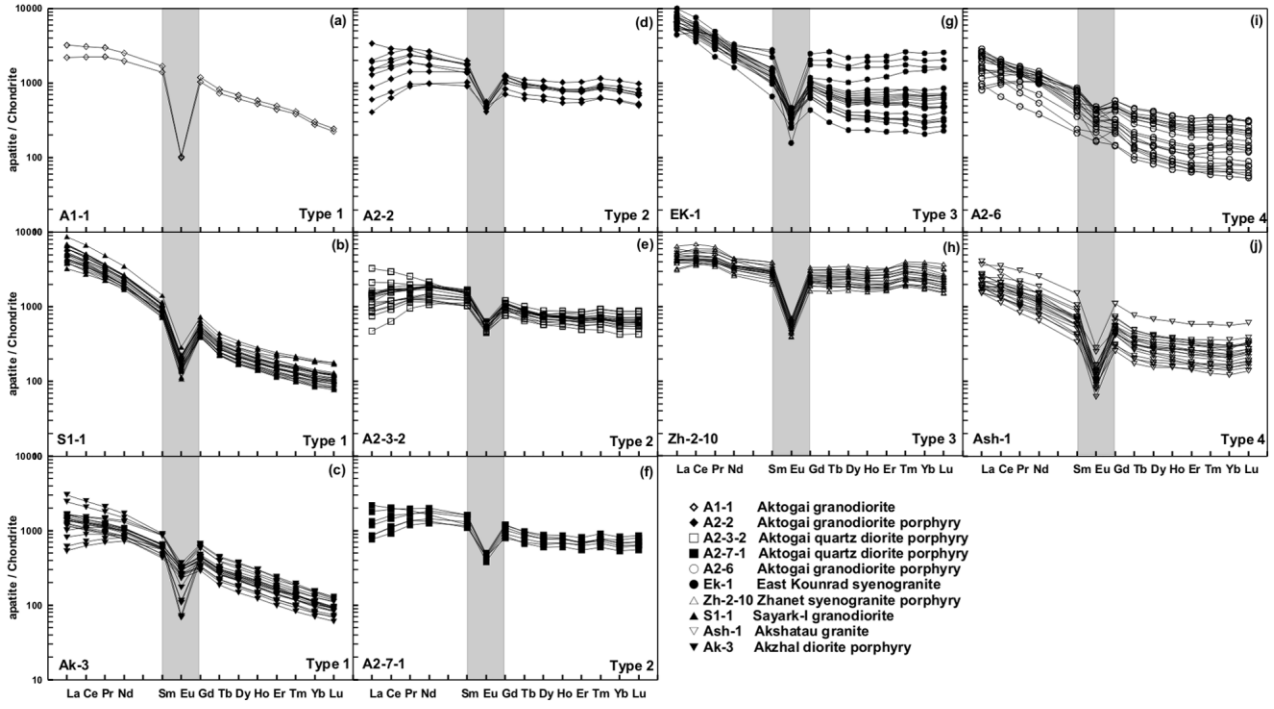

Fig. 5 Chondrite-normalized REE patterns of apatites. Chondrite REE values from Taylor and McLennan (1985).

Zh-2–10 (Zhanet), strong negative $(Eu/Eu^*)_N$, flat middle REE (MREE) and heavy REE (HREE), and distinct Nd depletion; and type 4, A2-6 (Aktogai) and Ash-1 (Akshatau), marked by right-inclined REE pattern with wide distributed content of REE, negative $(Eu/Eu^*)_N$, flat MREE and HREE (Fig. 5).

7. Discussion

7.1 Petrogenesis

7.1.1 The magma source character

A similar magmatic source is supported by the consistent concentrations of major and trace elements, and also REE patterns among Ek-1, Zh-2–1 and Zh-2–10 apatites from Mo-W deposits and among A2-2, A2-3-3 and A2-7-1 apatites from the Aktogai porphyry Cu deposit (Table 4). The relative identical ratios of F/Cl $(La/Yb)_N$ and $(Eu/Eu^*)_N$, and contents of Sr, Mn and Y in apatites between the skarn Cu deposit and porphyry Cu-Mo deposits, as well as between W-Mo deposits and Mo-W deposits, suggest close magma sources between the skarn Cu deposit and porphyry Cu-Mo deposits, and between W-Mo deposits and Mo-W deposits (Table 4).

High F/Cl ratios in apatites of Ek-1, Zh-2–1 and Zh-2–10 all from Mo-W deposits are likely due to remelting of sedimentary source rocks, which have experienced a relative enrichment of F and probable loss of Cl during weathering processes owing to the high solubility of Cl in aqueous solutions (Brehler & Fuge, 1974). Nonetheless, low F/Cl ratios in apatites of Ak-3 are likely related to high water content in magma reflected by great quantities of hornblendes, because Cl displays strong preference for the fluid phase compared with F (e.g. Candela, 1986; Boudreau & Kruger, 1990). The high value of Mn in apatite from both Mo-W deposits (Ek-1, Zh-2–1 and Zh-2–10) cannot be simply interpreted by the differentiation degree, because Mn content of apatite from Ek-1, Zh-2–1 and Zh-2–10 increases abruptly compared with other samples, and shows no increasing with differentiation among these three samples. Therefore, high content of Mn in apatite from Mo-W deposits is possibly contributed partly by the source of sedimentary rocks (Belousova *et al*., 2001).

The exceptional high oxidation of magma reflected by the $(Eu/Eu^*)_N$ in apatites of Aktogai porphyries and anhydrite inclusion in A2-6 apatite manifests that porphyry Cu-Mo deposit develops at a magmatic arc related to oceanic plate subduction, since arc magma usually shows the character of high oxidation state (Blevin & Chappell, 1992, 1995; Richards, 2003; Blevin, 2004; Imai, 2004).

7.1.2 The process of apatite crystallization

Hornblende and zircon are known to concentrate HREE (Arth, 1976; Pearce & Norry, 1979; Mahood & Hildreth, 1983; Fujimaki, 1986; Bea *et al*., 1994; Klein *et al*., 1997). Type 1 character of highest $(La/Yb)_N$ in apatites of A1-1, S1-1 and Ak-3 is likely produced by the crystallization of hornblende and/or zircon, which is in accordance with the apatite occurrence primarily occurring with hornblende or associated with zircon (Fig. 2a, e). Type 2 character in apatites of Aktogai porphyries A2-2, A2-3-2 and A2-7-1 with unique upward-convex LREE likely results from La-enriched mineral crystallization (possibly allanite), since no La-depletion is detected in these three porphyries. However, the distinct feature of Nd depletion in type 3 apatites of Ek-1 and Zh-2–10 both from Mo-W deposits primarily inherits the character of host rocks, while not that of the crystallization of Nd-enriched minerals such as monazite from the magma (Yurimoto *et al*., 1990), as no visible negative Nd anomaly is detected in apatite REE patterns normalized to host magma composition (Fig. 6). A variation of HREE concentrations in type 3 apatites of Ek-1 may suggest that apatite crystallization experiences a broad temperature range, which is consistent with the most evolved composition for Ek-1 with SiO_2 content of 76.2 wt%. Additionally, a relatively wide range of REE contents in type 4 apatites of A2-6 and Ash-1 may also suggest that apatite crystallizes under a wide temperature range. A2-6 as the latest porphyry may have been emplaced into a relatively hot environment, and Ash-1 have a relatively evolved composition with SiO_2 content of 70.3 wt%.

7.2 Metallogenesis

7.2.1 The redox state of rocks

The ratios of Eu^{2+}/Eu^{3+} and Ce^{3+}/Ce^{4+} in melt and possible mineral (apatite) are greatly dependent upon oxygen fugacity, bulk rock composition, temperature and possible pressure (Drake, 1975). Low oxygen fugacity results in high Eu^{2+}/Eu^{3+}, Ce^{3+}/Ce^{4+}, low Eu^{3+} content, but high Ce^{3+} concentration in melts (Sha & Chappell, 1999), possibly leading to limited Eu^{3+} but great Ce^{3+} partitioning into apatite, thus creating a strong negative Eu anomaly, while creating obvious positive Ce anomaly in apatite. It suggests that the extent of Eu and Ce anomaly in apatite may be used to infer the redox state of the magma.

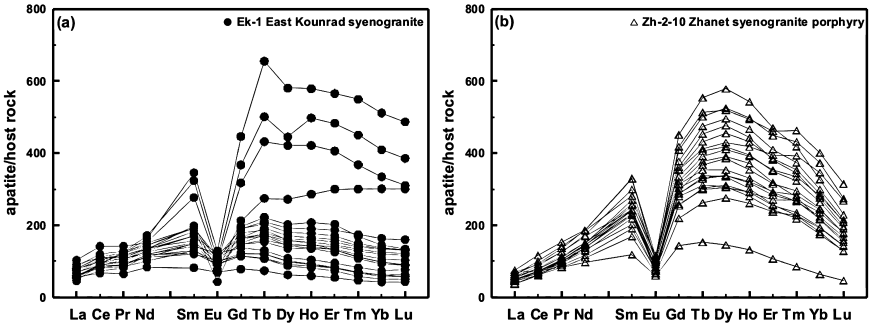

Fig. 6 Host rock-normalized REE patterns of apatites.

There are two different sites for Ca^{2+} in apatite, the sevenfold coordinated position ($^{VII}Ca^{2+}$) and ninefold coordinated position ($^{IX}Ca^{2+}$). REE^{3+} cations should couple with another ion to substitute Ca^{2+} in apatite (e.g. Ronsbo, 1989; Hughes *et al*., 1991; Fleet & Pan, 1995, 1997; Qin, 1997; Fleet *et al*., 2000). The opinions about the distribution of REE between the two distinct Ca positions in apatite are different. Cockbain and Smith (1967) proposed that REEs have no preference for either site. Urusov and Khudolozhkin (1974) argued that all REEs prefer $^{VII}Ca^{2+}$, while Borisov and Klevtova (1963) took the opposite viewpoint that all REEs prefer $^{IX}Ca^{2+}$. Further, LREEs were reported to display pronounced favor for $^{VII}Ca^{2+}$ (Hughes *et al*., 1991).

Both Eu and Ce have two ionic valences: Eu^{2+}-Eu^{3+} and Ce^{3+}-Ce^{4+}, respectively. The ionic radius of $^{VII}Ca^{2+}$, $^{IX}Ca^{2+}$, $^{VII}Eu^{2+}$, $^{IX}Eu^{2+}$, $^{VII}Eu^{3+}$, $^{IX}Eu^{3+}$, $^{VII}Ce^{3+}$ and $^{IX}Ce^{3+}$ are 0.106 nm, 0.118 nm, 0.120 nm, 0.130 nm, 0.101 nm, 0.112 nm, 0.107 nm and 0.196 nm, respectively (Shannon, 1976). Ce^{4+} has coordinations of sixfold, eightfold, tenfold and twelvefold, without any odd number coordinations (Shannon, 1976), which is required to substitute Ca^{2+} in apatite. The differences in ionic radius between Eu^{2+} and Ca^{2+} for the sevenfold and ninefold coordinations are:

$$\Delta r(\text{VII-1}) = \left|r(^{VII}Eu^{2+}) - r(^{VII}Ca^{2+})\right| = 0.014 \text{ nm},$$
$$\Delta r(\text{IX-1}) = \left|r(^{IX}Eu^{2+}) - r(^{IX}Ca^{2+})\right| = 0.012 \text{ nm},$$

and those between Eu^{3+} and Ca^{2+} for the sevenfold and ninefold coordinations are:

$$\Delta r(\text{VII-2}) = \left|r(^{VII}Eu^{3+}) - r(^{VII}Ca^{2+})\right| = 0.005 \text{ nm},$$
$$\Delta r(\text{IX-2}) = \left|r(^{IX}Eu^{3+}) - r(^{IX}Ca^{2+})\right| = 0.006 \text{ nm},$$

and those between Ce^{3+} and Ca^{2+} for the sevenfold and ninefold coordinations are:

$$\Delta r(\text{VII-3}) = \left|r(^{VII}Ce^{3+}) - r(^{VII}Ca^{2+})\right| = 0.001 \text{ nm},$$
$$\Delta r(\text{IX-3}) = \left|r(^{IX}Ce^{3+}) - r(^{IX}Ca^{2+})\right| = 0.0016 \text{ nm}.$$

REE substitutions in apatite follow the proximity principle, specifically, the less the radius difference, the easier the substitution. Apatite shows a marked preference for Eu^{3+} and Ce^{3+}, instead of Eu^{2+} and Ce^{4+}, as the ionic radius of Eu^{3+} is much closer to that of Ca^{2+} than Eu^{2+} for both Ca sites in apatite, and Ce^{3+} is nearly identical with Ca^{2+} in ionic radius at seven- or ninefold coordination sites. No odd number coordination for Ce^{4+} and nearly identical ionic radius between Ce^{3+} and Ca^{2+} suggest most Ce enter into apatite in the form of Ce^{3+} regardless of oxygen fugacity. That is why our results show no distinct difference for apatite Ce/Ce*, while there are obvious differences for apatite Eu/Eu* among samples, which indicate Eu anomaly in apatite could more effectively reflect redox state of the magma compared with Ce anomaly in apatite.

Three kinds of apatites with distinct redox states are identified based on Eu anomaly (Fig. 7). Apatite of A2-6 displays the most oxidized state, and apatites of A2-2, A2-3-2, A2-7-1, Ek-1 and Ak-3 show moderate oxidizing condition, while Ash-1, S1-1, Zh-2–10 and A1-1 apatites have a moderate reductive state (Fig. 7).

The anomaly of Eu in apatites of the Aktogai samples suggests that the early batholith A1-1 have the lowest oxygen fugacity. Samples of A1-1, porphyries A2-2, A2-7-1, A2-3-2, and A2-6 show an increasing trend of oxidizing degree with decreasing age, which is supported by the higher SO_3 in A2-6 apatites compared with other porphyries and the presence of anhydrite as mineral inclusion in A2-6 apatite.

A higher oxygen fugacity is observed in apatite from the rock associated with Cu-Mo mineralization than that from Mo-W deposit (Zh-2–10), skarn Cu deposit (S1-1) and W-Mo deposit (Ash-1). Actually it has been illustrated that porphyry Cu-Mo deposit is generated

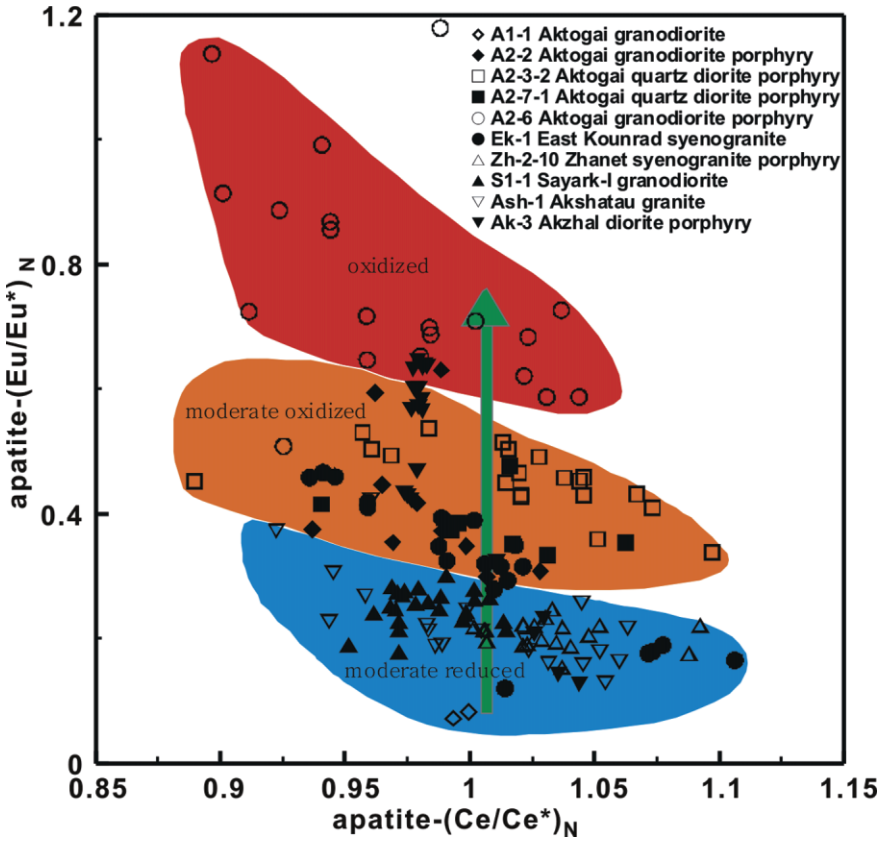

Fig. 7 Apatite Eu anomalies $(Eu/Eu^*)_N$ versus apatite Ce anomalies $(Ce/Ce^*)_N$; $Eu^*_N = (1/2)Sm_N+(1/2)Gd_N$, $Ce^*_N = (1/2)La_N+(1/2)Pr_N$.

from a highly oxidized magma, while Mo-W and W-Mo mineralization are produced by relatively reductive melts (e.g. Blevin & Chappell, 1992, 1995; Blevin, 2004). S1-1 from skarn Cu deposit exhibits a low redox state, likely caused by the wall rock of marine volcanogenic-carbonate and terrigenous molasses sediments. As to the two Mo-W deposits, higher redox state is identified in Ek-1 than in Zh-2–10, which agrees well with higher SO_3 content in apatite for Ek-1 (mean 0.36 wt%) than that for Zh-2–10 (mean 0.21 wt%).

7.2.2 The potential detectors to metallogenesis and ore types

Figure 8 shows some statistics between the element or ratio of elements in apatite. F/Cl ratios and F contents in apatites vary widely but show clear positive correlations (Fig. 8a), which may be a reflection of magmatic differentiation degree supported by whole rock SiO_2 content increasing from 58.8 to 76.2 wt%. Sr, Y and Mn contents in apatite are mainly related to degree of magmatic differentiation (Figs 3d and 4b, c). The $(La/Yb)_N$ and $(Eu/Eu^*)_N$ in apatites reflect the REE differentiation and redox state of the magma when apatite crystallizes. Different types of ore deposits are related to distinct differentiated magma, different oxidation of magma, and different resource rock, so different types of deposits display diverse characters of F, Cl, Mn, Sr, Y $(La/Yb)_N$ and $(Eu/Eu^*)_N$ in apatite (Fig. 8). Apatites from Mo-W deposits show high F content, F/Cl ratio, low Sr content and low $(Eu/Eu^*)_N$ ratio. Apatites from skarn Pb-Zn deposits display low content of F and Y, and high content of Cl and Sr. Apatites from porphyry Cu deposit are characterized by the high ratio of $(Eu/Eu^*)_N$. Apatites from skarn Cu deposit are distinct by high $(La/Yb)_N$. Apatites from W-Mo deposits exhibit low content of Sr, and low ratio of $(La/Yb)_N$ and $(Eu/Eu)_N$.

Therefore, contents of Sr, Mn, Y, maybe F, and ratios of F/Cl $(La/Yb)_N$ $(Eu/Eu^*)_N$ in apatites could be used to indicate magmatic differentiation, crystallization environment and ore deposit types (Fig. 8).

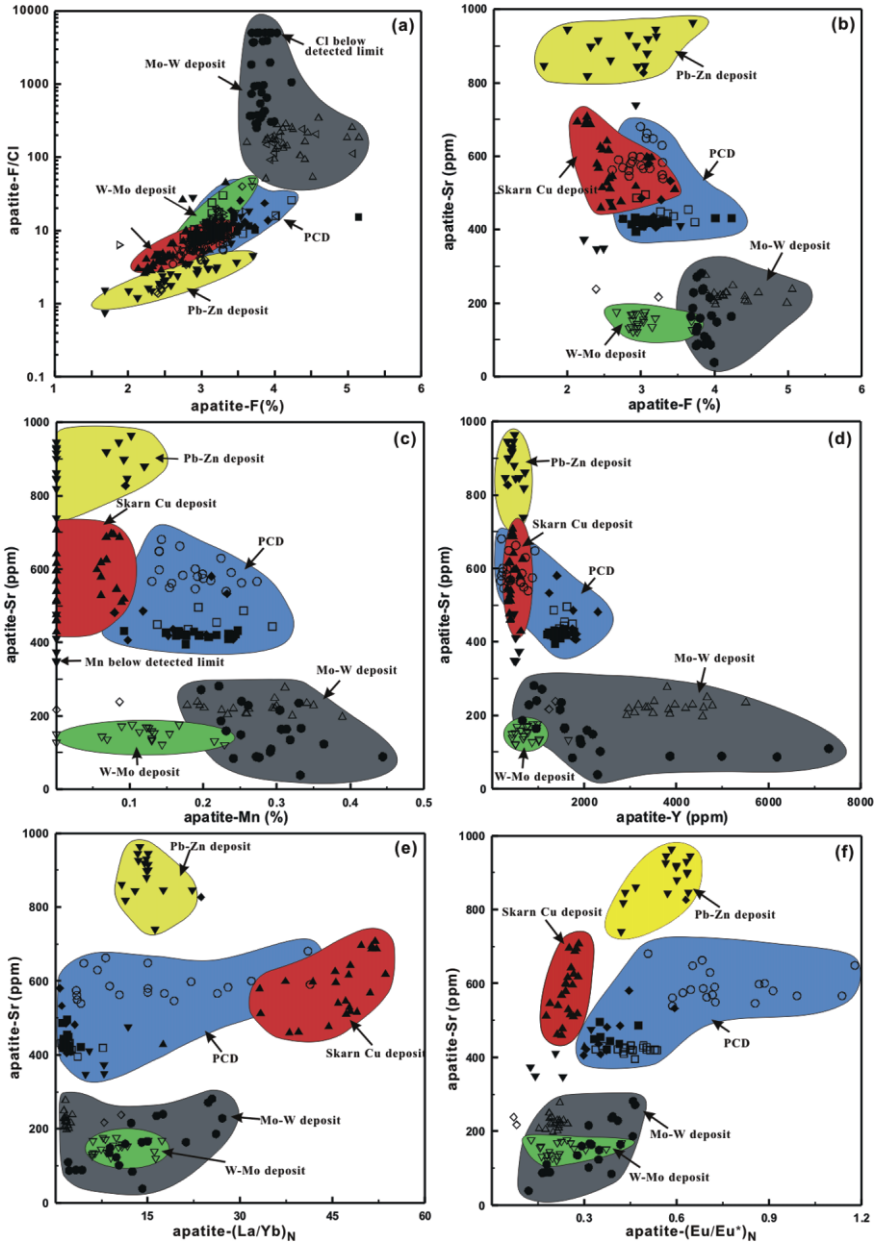

Fig. 8 Minor and trace element discrimination plots for apatite from Central Kazakhstan, fields of apatite composition from different types of deposit, proposed as discriminant plots, PCD is abbreviation of porphyry Cu-Mo deposit.

8. Conclusions

1 The highest F/Cl ratio and Mn content in apatites from Mo-W deposits are likely due to remelting of sedimentary source rocks, while the highest Cl content in apatite from Pb-Zn deposits probably indicates high water content in magma.

2 MnO, Sr and Y contents in apatites are mainly related to degree of magmatic differentiation.

3 High $(La/Yb)_N$ in apatites from type 1 result from crystallization of HREE-enriched minerals. Type 2 apatites with upward-convex LREE pattern are probably due to crystallization of La-enriched

minerals prior to apatite saturation in the source rock of magma. Nd depletion of type 3 apatites inherits the character from host magma. Wide distribution of REE contents in type 4 apatites are considered as a result of prolonged intervals of apatite saturation.

4 The slight negative Eu anomaly in A2-6 apatite indicates the most oxidized state, and moderate negative Eu anomaly in apatites of A2-2, A2-3-2, A2-7-1, Ek-1 and Ak-3 shows a moderate oxidizing condition, while strong Eu anomaly in Ash-1, S1-1, Zh-2–10 and A1-1 apatites reveals moderate reductive state.

5 Apatite geochemistry (such as F, Cl, Mn, Sr, Y $(La/Yb)_N$ and $(Eu/Eu^*)_N$) could be used to indicate magmatic differentiation, crystallization environment and ore deposit types.

Acknowledgments

This research was supported by the CAS Knowledge Innovation Project (Grant number kzcx2-yw-107) and the National 305 project of China (Grant number 2006BAB07B08). We would like to extend our gratitude to Dr. Qian Mao and Mr. Yuguang Ma for their assistance in EPMA analyses at the State Key Laboratory of Lithospheric Evolution of the Institute of Geology and Geophysics, Chinese Academy of Sciences. We thank Dr. Jinxiang Li, Dr. Dongmei Tang, Dr. Lei Chen, Mr. Junxing Zhao and Miss Pingping Liu for their kind help and valuable discussions. We gratefully thank two anonymous reviews and Chief Editor, Dr. Yasushi Watanabe, for their very stimulating comments and constructive suggestions, which have improved the manuscript in many aspects.

References

Apollonov, M. K. and Patalakha, E. I. (1981) History of geological evolution of the Paleozoides: Tectonic problems of Kazakhstan. Nauka, Almaty, 27–42.

Arth, J. (1976) Behavior of trace elements during magmatic processes-a summary of theoretical models and their applications. J. Res. US Geol. Surv., 4, 41–47.

Avdeev, N. T. (1984) Ophiolite zones and the geologic history of Kazakhstan from the mobilist standpoint: internat. Geol. Rev., 26, 995–1005.

Bea, F., Pereira, M. and Stroh, A. (1994) Mineral/leucosome trace-element partitioning in a peraluminous migmatite (a laser ablation-ICP-MS study). Chem. Geol., 117, 291–312.

Belousova, E. A., Griffin, W. L., O'Reilly, S. Y. and Fisher, N. I. (2002) Apatite as an indicator mineral for mineral exploration: trace-element compositions and their relationship to host rock type. J. Geochem. Explor., 76, 45–69.

Belousova, E. A., Walters, S., Griffin, W. L. and O'Reilly, S. Y. (2001) Trace-element signatures of apatites in granitoids from the Mt Isa Inlier, northwestern Queensland. Aust. J. Earth Sci., 48, 603–619.

Beskin, S. M., Larin, V. N. and Marin, Y. B. (1996) The Greisen Mo-W Deposit of Aqshatau, Central Kazakhstan. In Shatov, V., Seltmann, R., Kremenetsky, A., Lehmann, B., Popov, V. and Ermolov, P. (eds.) Granite-Related Ore Deposits of Central Kazakhstan and Adjacent Areas. Glagol Published House, St. Petersburg, 145–154.

Bhatnagar, V. (1969) Anion substitutions in lead apatites. Z. Anorg. Allgem. Chem., 367, 289–292.

Blevin, P. (2004) Redox and Compositional Parameters for Interpreting Granitoid Metallogeny of Eastern Australia: Implications for Gold-rich Ore Systems. Resour. Geol., 54, 241–252.

Blevin, P. and Chappell, B. (1992) The role of magma sources, oxidation states and fractionation in determining the granite metallogeny of eastern Australia. Trans. R. Soc. Edinb. Earth Sci., 83, 305–316.

Blevin, P. and Chappell, B. (1995) Chemistry, origin, and evolution of mineralized granites in the Lachlan fold belt, Australia; the metallogeny of I-and S-type granites. Econ. Geol., 90, 1604–1619.

Borisov, S. and Klevtova, R. (1963) The crystal structure of TR-Sr-apatite. J. Struct. Chem., 4, 575–577.

Boudreau, A. and Kruger, F. (1990) Variation in the composition of apatite through the Merensky cyclic unit in the western Bushveld Complex. Econ. Geol., 85, 737–745.

Brehler, B. and Fuge, R. (1974) Chlorine. In Wedepohl, K. H. (ed.) Handbook of geochemistry. Springer-Verlag, Berlin, II-2, 17A–17O.

Candela, P. (1986) Toward a thermodynamic model for the halogens in magmatic systems: an application to melt-vapor-apatite equilibria. Chem. Geol., 57, 289–301.

Chen, X. H., Qu, W. J., Han, S. Q., Eleonora, S., Yang, N., Chen, Z. L., Zeng, F. G., Du, A. D. and Wang, Z. H. (2010) Re-Os geochronology of Cu and W-Mo deposits in the Balkhash metallogenic belt, Kazakhstan and its geological significance. Geosci. Front., 1, 115–124.

Chu, M., Wang, K., Griffin, W., Chung, S., O'Reilly, S., Pearson, N. and Iizuka, Y. (2009) Apatite Composition: Tracing Petrogenetic Processes in Transhimalayan Granitoids. J. Petrol., 50, 1829–1855.

Claoue-Long, J. C., Sobolev, N. V., Shatsky, V. S. and Sobolev, A. V. (1991) Zircon response to diamond-pressure metamorphism in the Kokchetav massif, USSR. Geology, 19, 710–713.

Cockbain, A. and Smith, G. (1967) Alkaline-earth rare-earth silicate and germanate apatites. Mineral. Mag., 36, 411–421.

Coleman, R. (1989) Continental growth of northwest China. Tectonics, 8, 621–635.

Cooke, D. R., Hollings, P. and Walshe, J. L. (2005) Giant porphyry deposits: characteristics, distribution, and tectonic controls. Econ. Geol., 100, 801–818.

Degtyarev, K. E. (1999) Tectonic evolution of the early Paleozoic active margin in Kazakhstan. Transactions of GIN. Nauka, Moscow, 1–124 (in Russian).

Drake, M. (1975) The oxidation state of europium as an indicator of oxygen fugacity. Geochim. Cosmochim. Acta, 39, 55–64.

Farley, K. and Stockli, D. (2002) (U-Th)/He Dating of Phosphates: Apatite, Monazite, and Xenotime. Rev. Mineral. Geochem., 48, 559–577.

Fleet, M., Liu, X. and Pan, Y. (2000) Rare-earth elements in chlorapatite [$Ca_{10}(PO_4)_6Cl_2$]: Uptake, site preference, and degradation of monoclinic structure. Am. Miner., 85, 1437–1446.

Fleet, M. and Pan, Y. (1995) Site preference of rare earth elements in fluorapatite. Am. Miner., 80, 329–335.

Fleet, M. and Pan, Y. (1997) Rare earth elements in apatite: Uptake from H2O-bearing phosphate-fluoride melts and the role of volatile components. Geochim. Cosmochim. Acta, 61, 4745–4760.

Fujimaki, H. (1986) Partition coefficients of Hf, Zr, and REE between zircon, apatite, and liquid. Contrib. Mineral. Petrol., 94, 42–45.

Gleadow, A. J. W., Belton, D. X., Kohn, B. P. and Brown, R. W. (2002) Fission Track Dating of Phosphate Minerals and the Thermochronology of Apatite. Rev. Mineral. Geochem., 48, 579–630.

Harrison, T., Catlos, E. and Montel, J. (2002) U-Th-Pb dating of phosphate minerals. Rev. Mineral. Geochem., 48, 524–558.

Hasebe, N., Barbarand, J., Jarvis, K., Carter, A. and Hurford, A. (2004) Apatite fission-track chronometry using laser ablation ICP-MS. Chem. Geol., 207, 135–145.

Heinhorst, J., Lehmann, B., Ermolov, P., Serykh, V. and Zhurutin, S. (2000) Paleozoic crustal growth and metallogeny of Central Asia: evidence from magmatic-hydrothermal ore systems of Central Kazakhstan. Tectonophysics, 328, 69–87.

Henoc, J. and Tong, M. (1978) Automatisation de la microsonde. J. Microsc. Spectrosc. Electr., 3, 247–254.

Hsieh, P., Chen, C., Yang, H. and Lee, C. (2008) Petrogenesis of the Nanling Mountains granites from South China: constraints from systematic apatite geochemistry and whole-rock geochemical and *Sr–Nd* isotope compositions. J. Asian Earth Sci., 33, 428–451.

Hu, Z., Gao, S., Liu, Y., Hu, S., Chen, H. and Yuan, H. (2008) Signal enhancement in laser ablation ICP-MS by addition of nitrogen in the central channel gas. J. Anal. At. Spectrom., 23, 1093–1101.

Hughes, J. M., Cameron, M. and Mariano, A. N. (1991) Rare-earth-element ordering and structural variations in natural rare-earth-bearing apatites. Am. Miner., 76, 1165–1173.

Imai, A. (2002) Metallogenesis of porphyry Cu deposits of the western Luzon arc, Philippines: K-Ar ages, SO_3 contents of microphenocrystic apatite and significance of intrusive rocks. Resour. Geol., 52, 147–161.

Imai, A. (2004) Variation of Cl and SO_3 Contents of Microphenocrystic Apatite in Intermediate to Silicic Igneous Rocks of Cenozoic Japanese Island Arcs: Implications for Porphyry Cu Metallogenesis in the Western Pacific Island Arcs. Resour. Geol., 54, 357–372.

Ishihara, S. (1981) The granitoid series and mineralization. Econ. Geol., 75th Anniversary, 458–484.

Klein, M., Stosch, H. G. and Seck, H. A. (1997) Partitioning of high field-strength and rare-earth elements between amphibole and quartz-dioritic to tonalitic melts: an experimental study. Chem. Geol., 138, 257–271.

Korzhinskiy, M. (1981) Apatite solid solutions as indicators of the fugacity of HCl and HF in hydrothermal fluids. Geochem. Int., 3, 44–60.

Kröner, A., Windley, B. F., Badarch, G., Tomurtogoo, O., Hegner, E., Jahn, B. M., Gruschka, S., Khain, E. V., Demoux, A. and Wingate, M. T. D. (2007) Accretionary growth and crust formation in the Central Asian Orogenic Belt and comparison with the Arabian-Nubian shield. Geol. Soc. Am. Memoir, 200, 181–209.

Kudryavtsev, Y. K. (1996) The Cu-Mo Deposits of Central Kazakhstan. In Shatov, V., Seltmann, R., Kremenetsky, A., Lehmann, B., Popov, V. and Ermolov, P. (eds.) Granite-Related Ore Deposits of Central Kazakhstan and Adjacent Areas. Glagol Publishing House, St. Petersburg, 119–144.

Kutoglu, A. (1974) Structure refinement of the apatite $Ca_5(VO_4)_3(OH)$. Neues Jahrb. Mineral. Monatsh., 5, 210–218.

Li, G. M., Qin, K. Z. and Li, J. X. (2008) Geological features and and tectonic settings of porphyry copper deposits rounding the Balkhash region, central Kazakhastan, central Asia. Acta Petrol. Sinica, 24, 2679–2700 (in Chinese with English abstract).

Liu, Y., Gao, S., Hu, Z., Gao, C., Zong, K. and Wang, D. (2010) Continental and Oceanic Crust Recycling-induced Melt-Peridotite Interactions in the Trans-North China Orogen: U-Pb Dating, Hf Isotopes and Trace Elements in Zircons from Mantle Xenoliths. J. Petrol., 51, 537–571.

Liu, Y., Hu, Z., Gao, S., Gunther, D., Xu, J., Gao, C. and Chen, H. (2008) In situ analysis of major and trace elements of anhydrous minerals by LA-ICP-MS without applying an internal standard. Chem. Geol., 257, 34–43.

Mahood, G. and Hildreth, W. (1983) Large partition coefficients for trace elements in high-silica rhyolites. Geochim. Cosmochim. Acta, 47, 11–30.

McInnes, B. I. A., Farley, K. A., Sillitoe, R. H. and Kohn, B. P. C. (1999) Application of apatite (U-Th)/He thermochronometry to the determination of the sense and amount of vertical fault displacement at the Chuquicamata porphyry copper deposit Chile. Econ. Geol., 94, 937–947.

Mossakovsky, A., Ruzhentsev, S., Samygin, S. and Kheraskova, T. (1993) Central Asian fold belt: geodynamic evolution and history of formation. Geotectonics, 6, 3–33.

Munoz, J. (1984) F-OH and Cl-OH exchange in micas with applications to hydrothermal ore deposits. Rev. Mineral. Geochem., 13, 469–493.

Nash, W. P. (1984) Phosphate minerals in terrestrial igneous and metamorphic rocks. In Nriaguand, J. O. and Moore, P. B. (eds.) Phosphate minerals. Springer-Verlag, Berlin, 215–241.

Norman, M. D., Griffin, W. D., Pearson, N. J., Garciac, M. O. and O'Reilly, S. Y. (1998) Quantitative analysis of trace element abundances in glasses and minerals: A comparison of laser ablation inductively coupled plasma mass spectrometry, solution inductively coupled plasma mass pectrometry, proton microprobe and electron microprobe data. J. Anal. At. Spectrom., 13, 477–482.

Norman, M. D., Pearson, N. J., Sharma, A. and Griffin, W. L. (1996) Quantitative analysis of trace elements in geological materials by laser ablation ICPMS: instrumental operating conditions and calibration values of NISTglasses. Geostand. Newsl., 20, 247–261.

Omar, G., Johnson, K., Hickey, L., Robertson, P., Dawson, M. and Barnosky, C. (1987) Fission-track dating of Haughton astrobleme and included biota, Devon Island, Canada. Science, 237, 1603–1605.

Pearce, J. and Norry, M. (1979) Petrogenetic implications of Ti, Zr, Y, and Nb variations in volcanic rocks. Contrib. Mineral. Petrol., 69, 33–47.

Popov, V. S. (1996) Some Problems of Tectonics, Magmatism, and Metallogeny of Central Kazakhstan. In Shatov, V., Seltmann, R., Kremenetsky, A., Lehmann, B., Popov, V. and Ermolov, P. (eds.) Granite-Related Ore Deposits of Central Kazakhstan and Adjacent Areas. Glagol Publishing House, St. Petersburg, 109–116.

Qin, K. Z. (1997) Metallogenic systematis of the intracontinental magmatism in the southern Ergun Mo, Cu, Pb, Zn and Ag belt, Inner Mongolia, NE-China. Dr. Sci. Dissertation, Hokkaido University, Japan, 305p.

Qin, K. Z. (2000) Paleozoic Central-Asia orogeneses and metallogenese in Northern Xinjiang. Post-Doctoral research report. Institute of Geology and Geophysics, CAS, 195p (in Chinese with English abstract).

Qin, K. Z., Sun, S., Li, J. L., Fang, T. H., Wang, S. L. and Liu, W. (2002) Paleozoic epithermal Au and porphyry Cu Deposits in North Xinjiang, China: Epochs, Features, Tectonic Linkage and Exploration Significance. Resour. Geol., 52, 291–300.

Qin, K. Z., Zhang, L., Xiao, W., Xu, X., Yan, Z. and Mao, J. (2003) Overview of major Au, Cu, Ni and Fe deposits and metallogenic evolution of the eastern Tianshan Mountains, Northwestern China. In Mao, J., Goldfarb, R. J., Seltmann, R., Wang, D. H., Xiao, W. J. and Hart, C. J. (eds.) Tectonic Evolution and Metallogeny of the Chinese Altay and Tianshan. CERCAMS/NHM, London, IAGOD Guidebook Series, 10, 227–248.

Richards, J. (2003) Tectono-magmatic precursors for porphyry Cu-(Mo-Au) deposit formation. Econ. Geol., 98, 1515–1533.

Ronsbo, J. (1989) Coupled substitutions involving REEs and Na and Si in apatites in alkaline rocks from Ilimaussaq, South Greenland, and the petrological implications. Am. Miner., 74, 896–901.

Sallet, R. (2000) Fluorine as a tool in the petrogenesis of quartz-bearing magmatic associations: applications of an improved F-OH biotite-apatite thermometer grid. Lithos, 50, 241–253.

Sengor, A. M. C. (1993) Evolution of the Altaid tectonic collage and Palaeozoic crustal growth in Eurasia. Nature, 364, 299–307.

Sengor, A. M. C. and Natal'in, B. A. C. (1996) Turkic-type orogeny and its role in the making of the continental crust. Annu. Rev. Earth Planet. Sci., 24, 263–337.

Serykh, V. I. (1977) Paleozoic granitoid complexes and series of the Balqash region. Izv Akad Nauk Kazakh SSR, Ser. Geol., 3, 8–17.

Serykh, V. I. (1988) The succession and regular patterns of evolution of granitic rocks in polycyclic foldbelts (with an example from Central Kazakhstan). Geol. Geofiz., 9, 17–24.

Serykh, V. I. (1996) Granitic rocks of central Kazakhstan. In Shatov, V., Seltmann, R., Kremenetsky, A., Lehmann, B., Popov, V. and Ermolov, P. (eds.) Granite-related ore deposits of central Kazakhstan and adjacent areas. Glagol Publishing House, St Petersburg, 25–54.

Sha, L. K. and Chappell, B. W. (1999) Apatite chemical composition, determined by electron microprobe and laser-ablation inductively coupled plasma mass spectrometry, as a probe into granite petrogenesis. Geochim. Cosmochim. Acta, 63, 3861–3881.

Shannon, R. (1976) Revised effective ionic radii and systematic studies of interatomic distances in halides and chalcogenides. Acta Crystallogr. A, 32, 751–767.

Taylor, S. and McLennan, S. (1985) The continental crust: its composition and evolution. Blackwell Scientific Publications, Oxford, 1–328.

Treloar, P. J. and Colley, H. (1996) Variations in F and Cl contents in apatites from magnetite-apatite ores in northern Chile, and their ore-genetic implications. Mineral. Mag., 60, 285–301.

Urusov, V. and Khudolozhkin, V. (1974) An energy analysis of cation ordering in apatite. Geochem. Int., 11, 1048–1053.

Wilson, A., Sudarsanan, K. and Young, R. (1977) The structures of some cadmium "apatites" $Cd_5(MO_4)_3X$. II. The distributions of the halogen atoms in $Cd_5(VO_4)_3I$, $Cd_5(PO_4)_3Br$, $Cd_5(AsO_4)_3Br$, $Cd_5(VO_4)_3Br$ and $Cd_5(PO_4)_3Cl$. Acta Crystallogr. B Struct. Crystallogr. Crystal Chem., 33, 3142–3154.

Windley, B. F., Alexeiev, D., Xiao, W., Kroner, A. and Badarch, G. (2007) Tectonic models for accretion of the Central Asian Orogenic Belt. J. Geol. Soc., 164, 31–47.

Xiao, W. J., Windley, B. F., Badarch, G., Sun, S., Li, J. L., Qin, K. Z. and Wang, Z. H. (2004a) Palaeozoic accretionary and convergent tectonics of the southern Altaids: implications for the growth of Central Asia. J. Geol. Soc., 161, 339–342.

Xiao, W. J., Windley, B. F., Yuan, C., Sun, M., Han, C. M., Lin, S. F., Chen, H. L., Yan, Q. R., Liu, D. Y., Qin, K. Z., Li, J. L. and Sun, S. (2009) Paleozoic multiple subduction-accretion processes of the southern Altaids. Am. J. Sci., 309, 221–270.

Xiao, W. J., Zhang, L. C., Qin, K. Z., Sun, S. and Li, J. L. (2004b) Paleozoic accretionary and collisional tectonics of the eastern Tianshan (China): Implications for the continental growth of central Asia. Am. J. Sci., 304, 370–395.

Yakubchuk, A. (2004) Architecture and mineral deposit settings of the Altaid orogenic collage: a revised model. J. Asian Earth Sci., 23, 761–779.

Yakubchuk, A. S., Seltmann, R., Shatov, V. and Cole, A. (2001) The Altaids: tectonic evolution and metallogeny. Soc. Econ. Geol. Newsl., 46, 7–14.

Yakubchuk, A. S., Shatov, V. V., Kirwin, D., Tomurtogoo, O., Badarch, G. and Buryak, A. A. (2005) Gold and base metal metallogeny of the central Asian orogenic supercollage. Econ. Geol., 100, 1035–1068.

Yurimoto, H., Duke, E., Papike, J. and Shearer, C. (1990) Are discontinuous chondrite-normalized REE patterns in pegmatitic granite systems the results of monazite fractionation? Geochim. Cosmochim. Acta, 54, 2141–2145.

Zaitsev, Y. A. (1984) Evolution of geosynclines (the oval concentrically-zonal type). Nedra Publishing House, Moscow, 208 p (in Russian).

Zeitler, P., Herczeg, A., McDougall, I. and Honda, M. (1987) U-Th-He dating of apatite- A potential thermochronometer. Geochim. Cosmochim. Acta, 51, 2865–2868.

Zhu, C. and Sverjensky, D. A. (1992) F-Cl-OH partitioning between biotite and apatite. Geochim. Cosmochim. Acta, 56, 3435–3467.